986 *Macromolecules* **2010**, *43*, 986–1002
DOI: 10.1021/ma902199g

Macromolecules
ARTICLE

Advanced Monte Carlo Algorithm for the Atomistic Simulation of Short- and Long-Chain Branched Polymers: Implementation for Model H-Shaped, A_3AA_3 Multiarm (Pom-Pom), and Short-Chain Branched Polyethylene Melts

Chunggi Baig, Orestis Alexiadis, and Vlasis G. Mavrantzas*

Department of Chemical Engineering, University of Patras & FORTH-ICE/HT, Patras, GR 26504, Greece

Received October 8, 2009; Revised Manuscript Received December 2, 2009

ABSTRACT: We present a powerful connectivity-altering Monte Carlo (MC) algorithm for simulating atomistically detailed models of long- and short-chain branched polymers. Based on a mix of advanced and simple moves, the algorithm allows the robust simulation of chain systems with a variety of molecular architectures: H-shaped, A_3AA_3 multiarm (pom-pom), and short-chain branched (SCB) ones. For the H-shaped and A_3AA_3 architectures (**A** denotes the backbone and A the arm), in particular, the recently developed intermolecular double bridging (DB) move effecting a new bridging between the chain backbones or the branches of two different chains and the intramolecular double rebridging (IDR) move effecting a new bridging between two branches of the same chain [Karayiannis et al. *J. Chem. Phys.* **2003**, *118*, 2451] are shown to provide a robust sampling of their structural and conformational characteristics at the chain level. The double concerted rotation (d-CONROT) and H-shaped branch rebridging (H-BR) moves, on the other hand, which are important in relaxing internal degrees of freedom in the chain and the local structure around branch points, allow complete equilibration at the segmental level, which is prerequisite for the correct prediction of the volumetric and packing properties of the simulated systems. For the case of SCB polymers, a continuum configurational bias move for branched polymers (Br-CCB) has been designed capable of sampling changes in the atomic coordinates in the vicinity of branch points. Along with an effective implementation of the conventional end-bridging (EB) move, this has resulted in a powerful method for simulating SCB polymers with a prespecified distribution of branch points along the chain and given (i.e., fixed) number of carbon atoms per branch. To deal with polydispersity in the simulated systems, the algorithm is executed in a semigrand canonical ensemble by making use of the set of chain relative chemical potentials which for a bulk, linear system produces a uniform distribution of chain lengths [Pant and Theodorou *Macromolecules* **1995**, *28*, 7224]. Consistent with recent considerations by Ramos et al. [*Macromolecules* **2007**, *40*, 9640], two different chain length distributions should be simultaneously controlled in the course of the simulation for branched systems. The new, generalized MC algorithm is capable of thoroughly equilibrating model H-shaped, multiarm A_3AA_3, and SCB polymers at all length scales and adequately sampling fluctuations in their structural, volumetric, and conformational properties. Overall, we find that branched polymers are characterized by a stiffer conformation than linear analogues of the same total chain length. For the H-shaped and A_3AA_3 architectures, in particular, we have observed that each dangling arm exerts an entropically driven tensile force on the chain crossbar (the part of the chain between the two branch points), causing significant chain stretching. Our results extend the previous works of Karayiannis et al. [*J. Chem. Phys.* **2003**, *118*, 2451] on the simulation of H-shaped polymers to A_3AA_3 PE polymers and of Ramos et al. [*Macromolecules* **2007**, *40*, 9640] on the simulation of model ethylene−1-hexene copolymers to copolymers with longer α-olefinic side groups, such as the ethylene−1-octene and ethylene−1-decene ones.

1. Introduction

A major trend in polymer science today is to tune the material properties of the final products not just by blending chemically different monomers but by synthesizing new architectures and compositions of matter. This route is and continues to be enabled by innovations in catalyst and formulation technology and by recent advances in the development of experimental techniques for the precise control and characterization of the type and degree of chain branching. The result is the synthesis of polymers with some unique rheological properties, which has helped polymer companies realize new markets and increased market share derived from valuable cost/performance attributes. Typical examples include long-chain branched (LCB) polymers, SCB polyolefins, rings, dendrimers, hyperbranched polymers, stars, and star-shaped copolymers.[1−10] We mention, for example, that the presence of long chain branches in polyethylene (PE) of size comparable to that of the backbone leads to greater melt strength (extensional hardening) and higher low-shear viscosity but also to greater shear thinning.[11] For several other applications, on the other hand, it is desirable to have a polymer that has a lower crystallinity than linear polyethylene in the solid state without the presence of long chain branches along the main chain. This need led to the development of copolymers of ethylene with an α-olefin, which is usually butene, hexene, or octene (the use of α-olefins longer than propylene seems to enhance the reduction

*To whom correspondence should be addressed: e-mail vlasis@chemeng.upatras.gr; Ph +30-2610-997398; Fax +30-2610-965223.

 Published on Web 12/30/2009

of density at a given mole fraction).[2,6] These copolymers are produced at lower temperatures and pressures and thought to be random copolymers (the comonomer is randomly distributed along the chains). Their production is initiated by transition metal catalysts, particularly Ziegler or Philips type of catalyst, and the actual polymerization process can be done in either solution- or gas-phase reactors.[2] Usually, octene is the copolymer in solution phase while butene and hexene are copolymerized with ethylene in gas-phase reactors. At very low comonomer levels (1−2 mol %), the products are "medium density polyethylenes". At higher comonomer levels (from 2.5 to 3.5 mol %), the product is a "linear low density polyethylene" (LLDPE).[2,6] Therefore, LLDPE differs structurally from conventional LDPE because of the absence of long chain branching. It is further characterized by a narrower molecular weight distribution than conventional LDPE and, in combination with the linear structure, exhibits significantly different rheological properties. For example, during a shearing process, such as extrusion, LLDPE remains more viscous and therefore harder to process than an LDPE of equivalent melt index. In melt extension, LLDPE has lower viscosity at all strain rates. This means it will not strain harden the way LDPE does when elongated. As the deformation rate increases, LDPE demonstrates a dramatic rise in viscosity because of chain entanglement by long branches, a phenomenon which is not observed with LLDPE because the lack of long-chain branching allows the chains to "slide by" one another upon elongation without becoming entangled by branches. These explain why the rheological properties of LLDPE are summarized as "stiff in shear" and "soft in extension".[6] LLDPE has also higher tensile strength and higher impact and puncture resistance than LDPE.

From the point of view of applications, branched polymers such as LDPE and LLDPE are generally considered today to be very important materials and have penetrated almost all traditional markets for polyethylene. To keep their market share and, if possible, to increase it, polymer companies are in need today of computer capabilities that would enable the evaluation of new architectures and composition designs in advance of their synthesis. This could provide very reasonable parameter estimation for up-scale rheological simulations like those commonly practiced for fiber spinning, film blowing, and coating film processes using kinetic flow models.[12−16] Additionally, a computational screening and design-of-experiments can be undertaken to optimize the architecture and formulation of new resins for new products, through variation of backbone and branching architectures. In the long term, such a capability would enable the development of new commercial designs of *unexplored* polymer architectures according to future business needs.

From a theoretical point of view, the dynamics and rheological behavior of polymers as a function of their molecular architecture depend strongly on the topological interactions (entanglements) arising due to chain connectivity and uncrossability in concentrated solutions and melts[9,17] and how these are affected by chain branching. Today, it is believed that rather subtle movements of branch points in the melt dominate the special properties of LDPE and new metallocene-based LCB polyolefins. According to the tube model of the reptation theory, these phenomena can be typically represented in a mean-field approach by a curvilinear tube with a certain diameter (quantifying the strength of topological interactions). Chain motion is thus believed to be restricted only within the effective tube, thus giving rise to a curvilinear "snakelike" diffusion along the tube. Based on this "tube" approach of de Gennes and Doi−Edwards for linear polymers,[18] models of molecular dynamics have also been proposed to quantitatively explain the special rheology of model LCB structures, such as stars and H-shaped polymers.[9,10,13] Combined with flow-scale modeling, these molecular constitutive equations have also explained features such as vortex formation in converging flow, die swell, and injection stresses.[18]

An alternative approach to understanding structure−property relationships in polymer melts as a function of their molecular architecture is offered by molecular simulations.[19−21] This is because simulations (e.g., molecular dynamics methods) can concentrate on local branch point motion, effect of entanglement inhomogeneities, and tube deformation. Thus, in principle, they can provide fundamental information regarding what molecular mechanisms and interactions are responsible for the extraordinary rheological properties of branched polymers compared to linear melts.[22−24] In a second step, this information can be used to refine or parametrize macroscopic constitutive models based on the tube model idea, which are still phenomenological today (than molecularly based). However, molecular dynamics (MD) methods are plagued by the problem of long relaxation times characterizing chain motion and dynamics in branched polymers (compared to the intrinsic MD time scale, ∼2 fs per MD step[20]), since these grow exponentially with branch length.[17] If, on the other hand, one is interested in the study of the effect of chain branching on the static properties of the polymer (structural, thermodynamic, conformational, and topological), then one can resort to a nondynamic method. Monte Carlo, in particular, offers an excellent alternative for the simulation of the dense phases of polymers because it avoids tracking the actual dynamics of the system; in contrast to MD, in MC we rely on transition probabilities between different states of the simulated system. We do this by generating a Markov chain of configurations, which samples the probability distribution of the statistical-mechanical ensemble in which the simulation is carried out. Overall, MC involves three steps: (a) generation of an initial configuration, (b) trial of a randomly generated system configuration, and (c) evaluation of an "acceptance criterion" for the trial configuration and comparison to a random number to decide whether the trial configuration should be accepted or rejected. The acceptance criterion is usually formulated in terms of the potential energy change between trial (new) and existing (old) states and some other properties of the new and old configurations. Thanks in particular to the technique of "importance sampling", one can significantly accelerate sampling in a MC process by focusing preferentially on those states that make the most significant contributions to the configurational properties of the system. This is achieved by the design and efficient implementation of novel (clever and very drastic) moves, which cause significant changes in the set of atomic coordinates, thereby enhancing the performance of the algorithm not only at the level of local segmental motions but also (and more importantly) at the level of global properties (e.g., relaxation of end-to-end distance vectors).[25]

In the past two decades, a great deal of such ingenious MC algorithms schemes have been proposed and evaluated.[26−41] We mention, in particular, the development of the connectivity-altering end-bridging (EB) MC move,[30,31] the most efficient MC method available today for the fast equilibration of the long-length-scale characteristics of linear polymers of any chain length. The roots of the method can be traced back to the moves introduced in the 1980s in the form of "chain breaking" or "pseudokinetic" MC algorithms by Olaj and Lantschbauer,[42] which are capable of inducing drastic reconfiguration of large internal sections simultaneously along two different chains. The method relies on the geometric problem of trimer bridging, namely, how to connect a pair of dimers along two different chain backbones with a trimer, using predefined (i.e., preselected) values for all intervening bond lengths and bond angles.[35] It has been successfully applied so far to a variety of polymer systems both in the bulk[35] and at surfaces.[38,41] For example, it has allowed the simulation of linear polyethylene systems containing a very large (up to 6000) number

Scheme 1. Sketches of the Molecular Architectures Corresponding to H-Shaped, A_3AA_3, and SCB PE Chain Molecules

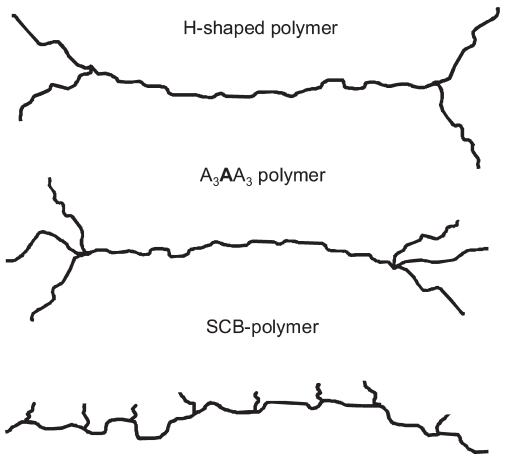

of united atoms per chain.[32] Fully equilibrated configurations obtained from the EB Monte Carlo simulations have also served as initial system configurations in subsequent MD simulations, thus enabling the study also of the dynamic properties of long-chain polymers.[43−45] An important extension of the end-bridging algorithm is the double-bridging algorithm, which has allowed the simulation of strictly monodisperse polymeric systems[33,34] and of H-shaped nonlinear polymer melts.[36] The H-shaped polymer is the simplest model structure for a branched polymer chain, yet capable of revealing the key role of branches on the dynamics of nonlinear polymer melts: the chain consists of a main backbone which connects two branch points (or junctions), from each one of which two dangling arms (i.e., branches) emanate (see Scheme 1). It is also a structure which can be simulated by the double-bridging Monte Carlo algorithm through a proper redesign of the move. To enable sampling of atomic coordinates in the vicinity of branch points, a double concerted rotation (d-CONROT) and a new move termed H-shaped branch rebridging (H-BR) have been further introduced.[36] In this work, we apply this advanced MC algorithm to simulate in detail a long H-polymeric system; we further extend it to a model A_3AA_3 polymer where three (instead of two) arms emanate from each of two branch points (see Scheme 1). In addition to the simulations of these two long-chain branched architectures (H-shaped and A_3AA_3), we also introduce and test here a new MC scheme for short-chain branched (SCB) polymers representative of LLDPE melts. The interest in this architecture comes from the commercial importance of the corresponding class of products (synthesized by using either Ziegler−Natta or metallocene catalysts) because they offer a better control on properties such as density, rigidity, hardness, and permeability.[6] To this, a new configurational-bias MC algorithm has been developed (termed Br-CCB here) capable of sampling fluctuations in the conformation of the short branches along the main-chain backbone. The move is similar to the br-CBMC proposed by Ramos et al.[40] for the simulation of SCB polyolefins (ethylene−1-hexene copolymers), but we have further allowed here the branch point to move along the chain backbone, a feature which allows sampling fluctuations also on the number of carbon atoms between successive branches along the chain. This is very important, since most SCB polymers synthesized by plastic companies are characterized by a certain degree of polydispersity not only in the total chain length but also in the interbranch spacing. As we will see in the next sections of this paper, the combination of the Br-CCB algorithm with the rest of the moves developed for H-shaped polymers (e.g., EB, d-CONROT, reptation, DB, IDR, and H-BR) results in an extremely efficient MC method for the simulation of SCB polymers of a prespecified branch length, branch-to-branch chain length distribution, and backbone (or total chain length) distribution.

The paper is organized as follows: In section 2, we discuss in due detail the molecular model employed in the present MC simulations, the types of model systems simulated, and the simulation method. We show how the various moves are implemented for H-shaped, A_3AA_3, and SCB polymer architectures, we provide schematics for all moves, we discuss the corresponding Metropolis criteria, and we report some technical details related to algorithm implementation and execution. The types of the simulated model systems and their microstructure (type and degree of chain branching) are discussed in section 3. In section 4 we present detailed results for the structural, thermodynamic, volumetric, and packing properties of all simulated systems and analyze their dependence on molecular architecture. The paper concludes with section 5 summarizing the important findings of this work and discussing future plans. An important point to make here is that although we have restricted ourselves to only three types of branched polymers (H-shaped, A_3AA_3, and SCB), the developed MC scheme is more general and can be extended (almost straightforwardly) to treat a number of other, more complex branched structures, such as stars, treelike dendrimers, and hyperbranched polymers.

2. Molecular Model and Simulation Method

All molecular simulations executed in this work have been carried out with the well-known TraPPE united-atom potential model,[46] according to which end methyl units (CH_3) and internal methylene (CH_2) and methyne (CH) groups along a chain are treated as individual but different interacting sites. Neighboring sites along the chain are held at a fixed distance equal to 1.54 Å. A harmonic potential is assumed to govern bond angle fluctuations around their equilibrium value, using different parameter values for the three different sets of angles ($CH_x-CH_2-CH_y$, $CH_x-CH-CH_y$, and CH_x-C-CH_y with x and y equal to 2 or 3) along a branched PE chain. A four-term cosine series was assumed to describe torsional angles, with different values for the expansion coefficients referring to the three different kinds ($CH_x-CH_2-CH_2-CH_y$, $CH_x-CH_2-CH-CH_y$, and $CH_x-CH_2-C-CH_y$ with x and y equal to 2 or 3) of dihedrals. Regarding nonbonded interactions (interactions between atoms separated by more than three bonds along the same chain or interactions between atoms belonging to different chains), a standard two-parameter 12−6 Lennard-Jones (LJ) potential was employed which differentiates between CH_3, CH_2, and CH units and in which cross-correlations are described by the standard Lorentz−Berthelot mixing rules, namely $\varepsilon_{ij} = (\varepsilon_i\varepsilon_j)^{1/2}$ and $\sigma_{ij} = (\sigma_i + \sigma_j)/2$, where ε_i and σ_i denote the energy and size parameters, respectively, of atom type i. The cutoff distance for the nonbonded interactions was chosen equal to $2.5\sigma_{ij}$; accordingly, the long-range correction to the total LJ energy was obtained by calculating separately (and then summing up) the contributions from the six different types of interaction (CH−CH, CH_2-CH_2, CH_3-CH_3, $CH-CH_2$, CH_3-CH_2, and $CH-CH_3$). All details of the molecular model (which, by treating end methyls and internal methylene and methyne groups as different sites, is characterized by increased predictive capability) are given in Table 1. The simulations were executed in a cubic simulation cell subject to periodic boundary conditions along all three (x, y, and z) directions.

As mentioned above, the present work has been motivated by recent advances in MC simulations for chain systems, which today can be calibrated using a variety of appropriate criteria and geometric methods to overcome the bottlenecks faced by molecular dynamics methods in simulations of dense polymer systems

Table 1. Atomistic Potential Model Used in the Simulations of Linear and Branched Polyethylene Melts

interaction type	potential function	model parameters
bond length		l_{eq} = 1.54 Å
bond bending	$U_{ben}(\theta) = \frac{1}{2}k_\theta(\theta-\theta_{eq})^2$	k_θ = 124.188 kcal/(mol rad^2) θ_{eq} = 114° for $CH_x-CH_2-CH_y$ θ_{eq} = 112° for $CH_x-CH-CH_y$ θ_{eq} = 109.47° for CH_x-C-CH_y
bond torsional	$U_{tor}(\phi) = \sum_{m=0}^{3} a_m(\cos\phi)^m$	a_0 = 2.0071, a_1 = 4.0122, a_2 = 0.27105, a_3 = −6.2895 (kcal/mol) for $CH_x-CH_2-CH_2-CH_y$ a_0 = 0.78542, a_1 = 1.7787, a_2 = 0.44454, a_3 = −3.5076 (kcal/mol) for $CH_x-CH_2-CH-CH_y$ a_0 = 0.91670, a_1 = 2.7503, a_2 = 0, a_3 = −3.6664 (kcal/mol) for $CH_x-CH_2-C-CH_y$
nonbonded Lennard-Jones	$U_{LJ}(r) = 4\varepsilon_{ij}\left[\left(\frac{\sigma_{ij}}{r}\right)^{12}-\left(\frac{\sigma_{ij}}{r}\right)^{6}\right]$	σ = 3.75 Å, ε = 0.19475 kcal/mol for CH_3 σ = 3.95 Å, ε = 0.09141 kcal/mol for CH_2 σ = 4.68 Å, ε = 0.01987 kcal/mol for CH

Table 2. Percent Acceptance Rates (Mix Ratio) of the MC Moves Employed in the Simulations of the Linear, H-Shaped, A_3AA_3, and SCB Polymers

MC moves[a]	L_1072	H_512_140	A_512_140	SCB_36 × 22_35 × 8	SCB_48 × 16.5_47 × 6
reptation[b]	8.0 (10)	8.1 (12)	8.2 (12)	7.7 (10)	7.2 (10)
rotation	18.0 (2)			17.4 (5)	17.3 (5)
flip	78.4 (6)	78.6 (5)	78.4 (8)	77.9 (5)	77.8 (5)
CONROT	8.5 (32)	8.3 (20)	8.5 (26)	8.6 (20)	8.5 (20)
d-CONROT		0.004 (4)	0.019 (7)	0.55 (19)	1.7 (19)
EB	0.16 (49)			0.17 (25)	0.16 (25)
DB		7.5×10^{-4} (33)	7.8×10^{-4} (27)		
IDR		6.0×10^{-4} (18)	6.8×10^{-4} (19)		
H-BR		0.008 (7)			
CCB				22.8 (8)	29.3 (8)
Br-CCB				0.097 (7)	0.22 (7)
VF	2.4 (1)	3.8 (1)	3.8 (1)	4.3 (1)	4.2 (1)

[a] CONROT: concerted rotation; d-CONROT: double concerted rotation; EB: end-bridging; DB: double bridging; IDR: intramolecular double rebridging; H-BR: H-shaped branch rebridging; CCB: continuum configurational bias for linear chains; Br-CCB: continuum configurational bias for branched chains; VF: volume fluctuation. [b] Standard reptation move for linear polymers and X-reptation move for branched polymers.

consisting of long chains. Building up, in particular, on recently introduced advanced moves, we present a composite method capable of simulating both long- and short-chain branched polymer architectures of a prespecified distribution of branch points, branch lengths, and interbranch spacing. The method relies on a suitable combination of traditional moves with improved variants of some newly developed chain connectivity altering ones and integrates them into a composite algorithm that is shown to provide a robust sampling of linear, H-shaped, A_3AA_3, and SCB polymers. The traditional moves include end-mer rotation, flip, reptation, X-reptation, and CONROT. The advanced moves include end-bridging (EB), double bridging (DB), d-CONROT, intramolecular double rebridging (IDR), continuum configurational bias for branched chains (Br-CCB), and H-shaped branch rebridging (H-BR). Most of them have already been developed and successfully implemented in simulations of a number of polymer systems: strictly monodisperse linear, H-shaped, triarm stars, mixtures of linear and triarms stars, and SCB polyolefins (ethylene−1-hexene copolymers). We have redesigned them here so that they can be employed in simulations of branched PE melts with an even broader variety of molecular architectures. We discuss this in detail in the next paragraphs of this section for all moves except end-mer rotation, reptation, and flip which are rather simple, and their implementation for branched polymers does not present a serious challenge. Regarding SCB polyolefins, in particular, we mention that in the past these have also been simulated by Ramos et al.[40] through a similar set of MC moves. Despite certain similarities between the two works, the code developed here differs in the following aspects: (a) Ramos et al.[40] simulated model systems corresponding only to ethylene−1-hexene copolymers. Here we address SCB polymers with longer olefinic side groups, corresponding to ethylene−1-octene and ethylene−1-decene copolymers. (b) For the equilibration of short arms, Ramos et al.[40] made use of the br-CBMC move. Here we make use of a modified version of this move (we call this Br-CCB), since we further allow the branch point to move along the main chain backbone prior to regrowing, in order to sample also fluctuations in the interbranch spacing. (c) To enhance the sampling of phase space near branch points, we further make use of the so-called d-CONROT move. (d) Lastly, our algorithm employs a standard formulation of the EB move, similar to the variant adopted for linear chains but slightly modified in order to account for the presence of branches; supplemented with a generalized reptation move, this move is found to be very efficient for the convergence of global properties of the architecturally realistic polymers simulated here or for equilibrating truly large systems, as its acceptance rate is comparable to that of linear molecules (see Table 2).

X-Reptation. This move is a generalization of the traditional and simple reptation move where one end of a randomly selected chain is cut off and reattached to the other end, with a fixed bond length and/or bond angle. By contrast, in the X-reptation move, two chains are randomly selected. Then, an end atom of a linear or branched chain is cut off from one of them and attached to the other end of the same chain or to any of the two ends of the other chain. Thus, in addition to displacing chains in space, this move induces polydispersity.

End-Bridging for SCB Systems (SCB-EB). The X-reptation move has been supplemented with the standard version of the end-bridging move[31] (slightly reformulated here to take into account the presence of branches along the chain) in order to enhance the performance of the algorithm at the level of global properties (e.g., end-to-end distance vectors). The move is realized by randomly selecting two chains in the melt and then allowing the end of one of them to attempt a trimer bridging with an internal backbone atom of the other chain, of course taking into account all restrictions imposed by the allowed values of the branch-to-branch and total (or backbone) molecular lengths.

Scheme 2. Schematic Representation of the Continuum Configurational Bias (Br-CCB) Monte Carlo Move Adopted in the Simulations of SCB Polymers

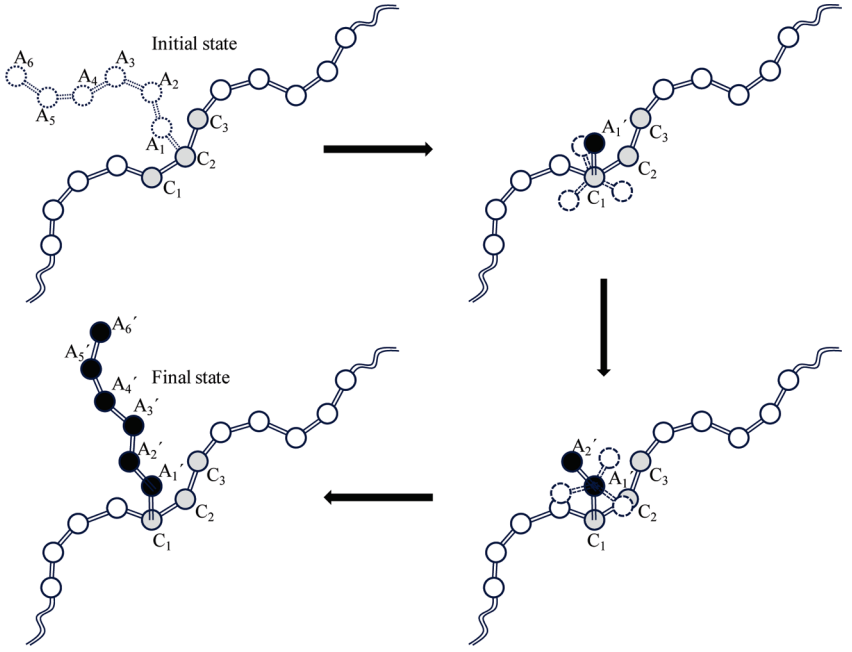

Continuum Configurational Bias for Branched Polymers (Br-CCB). Br-CCB is a modified version of the classical continuum configurational bias (CCB) Monte Carlo move developed[29] by de Pablo et al.[26] and Siepmann and Frenkel[27] based on the original Rosenbluth−Rosenbluth idea[47] of configurational bias in polymer lattice models. We have reformulated it here for equilibrating short chain branches along the main chain backbone by rebuilding (regrowing) all segments of the branch in a biased way. The move consists of the following three steps:

(a) First, a chain and a branch point (C2) along its contour are randomly selected, and the entire branch (A1 through A6) is excised, as schematically depicted in Scheme 2.

(b) Next, a new branch-point position adjacent to the original one (C2) [i.e., either on its left (C1) or on its right (C3)] is chosen along the backbone for the regeneration of the excised branch, and a step-by-step regeneration of all branch atoms is attempted in a biased fashion. According to this, the bond-bending and bond-torsional angles for each new atom to be generated are chosen with a weight proportional to their normalized Boltzmann factors. The total number, N_{dis}, of possible new states is taken to be equal to six, which was seen to be optimal for the systems considered here. For each of these six new possible positions (illustrated by dashed-line spheres in Scheme 2), the total system energy is calculated (involving only the nonbonded interaction), and the selection of the final new position is based on the following probability:

$$P_i = \frac{\exp\left(-\frac{U_{nb}^{(i)}}{K_B T}\right)}{\sum_{j=1}^{N_{dis}} \exp\left(-\frac{U_{nb}^{(i)}}{K_B T}\right)} \quad (1)$$

where $U_{nb}^{(i)}$ denotes the sum of the nonbonded interaction energy of the regrown atom at the prospective position i with all other atoms in the system. This process is repeated for all the N_{cut} atoms (A1 through A6) in the excised branch until a full trial configuration of the whole branch is created (A1′ through A6′).

(c) Lastly, all the bias introduced in the regeneration process is removed by adding a correction term (the Rosenbluth weight $W^{old \rightleftharpoons new}$) in the acceptance criterion as follows:

$$p_{acc} = \min\left[1, \frac{W^{new \rightarrow old} \exp\left[-\frac{U_{nb}^{new}}{K_B T}\right]}{W^{old \rightarrow new} \exp\left[-\frac{(U_{nb}^{old})}{K_B T}\right]}\right] \quad (2)$$

where the weight of the regrown branch is given by the product of the weights of the individual segments:

$$W^{old \rightarrow new} = \prod_{i=1}^{N_{cut}} P_i \quad (3)$$

In the above, $W^{old \rightarrow new}$ is determined from the solution of the reverse problem while U_{nb}^{old} and U_{nb}^{new} denote the total nonbonded interaction energy with the old (A1 through A6) and the new (A1′ through A6′) configurations of the whole branch, respectively.

Br-CCB allows sampling new configurations for the degrees of freedom associated with short branches along the chain. In addition, it induces fluctuations (within a prespecified interval) to the locations of branch points (and thus to the branch−branch distance). As we explained in the Introduction, this is very significant, since most SCB polylefins synthesized by polymer industries are characterized by a certain degree of polydispersity not only in the total chain length but also in the interbranch spacing.

Double Concerted Rotation (d-CONROT). d-CONROT is a generalization of the standard concerted rotation (CONROT) MC move[28] designed to induce large-scale system rearrangements near branch points; it is applicable to all types of branched polymers: H-shaped, A_3AA_3, and SCB ones. Scheme 3 illustrates its basic concepts. The move

Scheme 3. Schematic Representation of the Double Concerted Rotation (d-CONROT) Monte Carlo Move Adopted in the Simulations of H-Shaped, A_3AA_3, and SCB Polymers

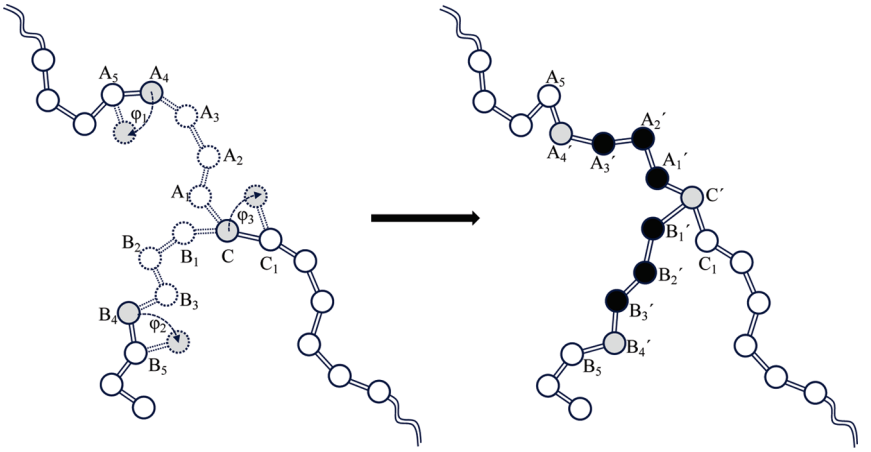

Scheme 4. Schematic Representation of the Intermolecular Double Bridging (DB) Move, Applied to Chain Backbones (a) or to Chain Branches (b), in Monte Carlo Simulations of H-Shaped and A_3AA_3 Polymers

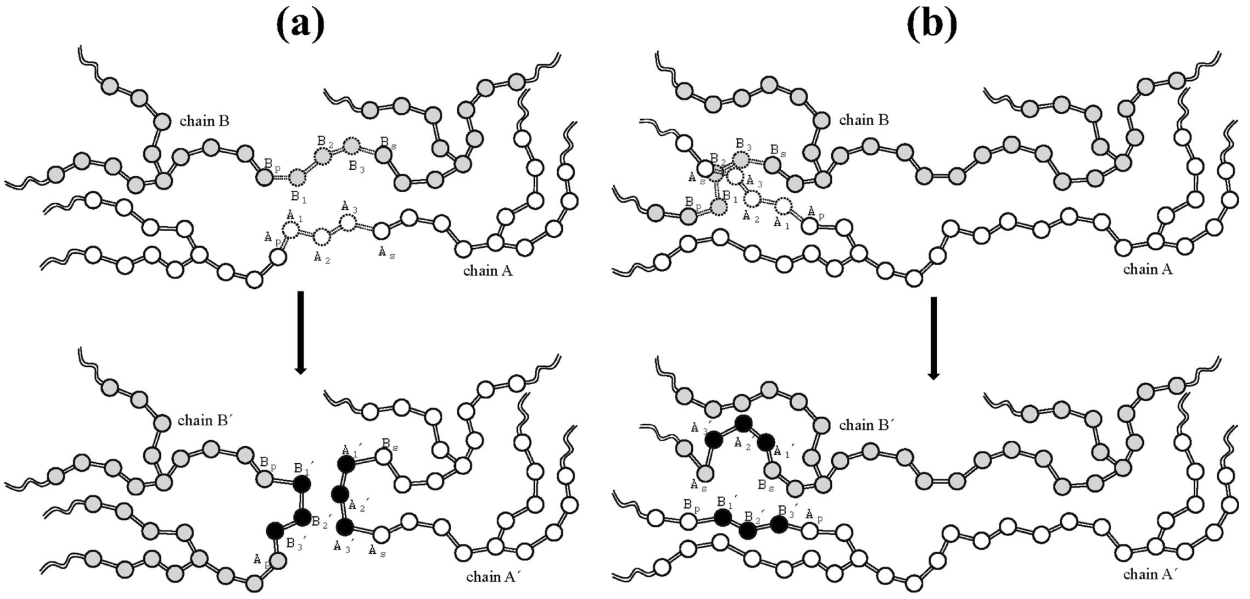

is initiated by removing two trimer sets (A1−A2−A3, B1−B2−B3) connected to a branch point (C) and by driving the two atoms (A4, B4) neighboring the removed trimers and the branch point (C) to new positions (A4′, B4′, C′), by altering the torsion angles (φ_1, φ_2, φ_3) within prescribed bounds ($-\delta\varphi_{max}$, $\delta\varphi_{max}$) ($\delta\varphi_{max} = 10°$ has been used in this work). Given the new coordinates of the three driven atoms (A4′, B4′, C′), the geometric problem of trimer bridging is solved simultaneously two times: one for the new construction connecting atoms A4′ and C′ through the A1′−A2′−A3′ trimer, and another for the new construction connecting atoms B4′ and C′ with the B1′−B2′−B3′ trimer. The bridging process takes place in such a way that the bonds of the altered segments (C1−C′−A1′−A2′−A3′−A4′−A5 and C1−C′−B1′−B2′−B3′−B4′−B5) preserve their equilibrium lengths, given a set of preselected values for all bond-bending angles involved in the move. The complete description of the move can be found in the papers by Dodd et al.[28] and Karayiannis et al.[36] Also reported in these works is the detailed expression for the acceptance criterion of the move, which in addition to the relevant Boltzmann factors includes the number of geometric solutions and the Jacobian determinants for the transformation from the set of Cartesian coordinates to the set of generalized coordinates employed in the geometric constructions; otherwise, the condition of detailed balance is not satisfied.

Double Bridging (DB) and Intramolecular Double Rebridging (IDR). The chain connectivity-altering double-bridging and intramolecular double rebridging MC moves (DB and IDR, respectively) are based on the formation of two bridging trimers between four properly chosen atoms along two selected chains; in the past, they have been formulated only for linear and H-shaped polymers.[33,34,36] We have extended their formulation here to multiarm A_3AA_3 (pom-pom) polymers. Like their predecessors, this has involved again the reconstruction of two bridging trimers between four properly chosen atoms along two selected A_3AA_3 chains. A schematic illustration of the DB move for H-shaped polymers before and after acceptance is presented in Scheme 4a (for a double-bridging between two chain backbones) and Scheme 4b (for a double-bridging between two branches). According to Scheme 4b, for example, DB is initiated by randomly selecting two branches [one from each chain

Scheme 5. Schematic Representation of the Intramolecular Double Rebridging (IDR) Monte Carlo Move Adopted in the Simulations of H-Shaped and A_3AA_3 Polymers

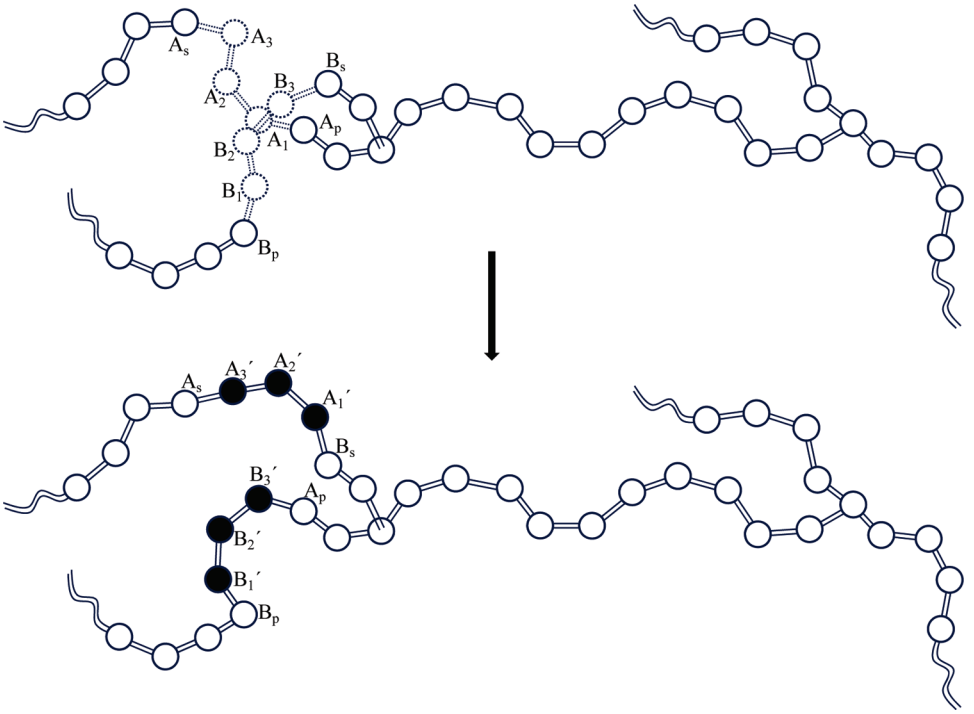

(A, B)] and picking an internal atom from each branch (Ap, Bp) which will be involved in the primary bridging. Next, the trimer set of three consecutive atoms adjacent to atom Bp, namely (B1−B2−B3), is excised, and the primary bridging between atoms Ap and Bp takes place by constructing a new conformation of the trimer, i.e., (B1′−B2′−B3′). Finally, the secondary bridging is realized between atom Bs lying next to the deleted trimer (B1−B2−B3) of chain B and atom As of chain A. This is implemented by abstracting the trimer (A1−A2−A3) connecting atoms Ap and As of chain A originally and by re-forming a new trimer configuration (A1′−A2′−A3′) to bridge atom As with atom Bs. A similar procedure is employed when DB is applied to chain backbones (Scheme 4a). As seen in Scheme 4, after a DB move has been accepted, the new chain conformations (A′, B′) are dramatically different from the old ones (A, B).

The implementation of the IDR algorithm is conceptually the same as of the DB move, except for the following differences: (a) it involves only a single chain, and (b) it allows for bridgings only between branches. We illustrate the IDR move in Scheme 5. For example, after a proper selection of two internal atoms (Ap, Bp) along two different branches in the same chain, the primary bridging is initiated by permitting atom Ap to attack atom Bp. The move proceeds by abstracting trimer (B1−B2−B3) next to atom Bp and constructing a new trimer (B1′−B2′−B3′) to bridge Ap with Bp. The IDR move is completed by invoking the secondary bridging so as to maintain chain connectivity and preserve the continuity of branches. The secondary bridging is accomplished by extracting the trimer (A1−A2−A3) adjacent to atom Ap and bridging atoms As and Bs with a new trimer (A1′−A2′−A3′). The acceptance criteria of the two moves (DB and IDR) have been discussed in detail by Karayiannis et al.[36]

H-Shaped Branch Rebridging (H-BR). Like DB and IDR, this move had been designed in the past only for simulations with H-polymers;[36] here, we have implemented it also for simulations with A_3AA_3 polymers. As shown in Scheme 6, it relies upon the solution of the geometric problem of trimer bridging, but two bridgings are required in the case of A_3AA_3 polymers (instead of one in the case of H-shaped ones). According to Scheme 6, the H-BR move begins by choosing one of the two branch points (e.g., atom A in Scheme 6) in a randomly selected chain and an atom four bonds apart from the branch point along the backbone or one of the neighboring branches (e.g., Ap in Scheme 6). After that, a trimer (e.g., A1′−A2′−A3′) between the branch point and the selected atom is excised and rebridged to a newly selected branch point (e.g., Bp). Therefore, depending on the movement direction of the branch point, the length of each branch and the backbone of an H-shaped or A_3AA_3 chain may increase or decrease; for example, for the case shown in Scheme 6, the length of the branch containing atom Bp is to be shortened and the backbone length to be lengthened after acceptance of the move, while the length of the branch containing the trimer (A1−A2−A3) remains constant. The acceptance criterion of the H−Br move has been presented in ref 36.

3. Systems Studied and Their Microstructure

Using the MC algorithm discussed in the previous section along with the TraPPE molecular model described in Table 1, a number of linear and branched PE melts of various molecular architectures have been simulated. The molecular lengths of the systems were carefully chosen so as to be characterized by the same number of carbon atoms along their longest linear dimension, and they include the following: (a) a linear PE melt containing on the average 792 carbon atoms per chain (denoted as L_792 here), (b) an H-shaped PE melt containing on the average 512 carbon atoms along the main chain backbone and 140 carbon atoms along each one of its four arms (we denote this as H_512_140), (c) an A_3AA_3 PE melt containing on the average 512 atoms along the main chain backbone and 140 carbon atoms along each one of its six arms (we denote this as A_512_140), and (d) a SCB PE melt containing on the average 792 carbon atoms along the main backbone and 48 short branches, each of which is

Scheme 6. Schematic Representation of the H-Shaped Branch Rebridging (H-BR) Monte Carlo Move Adopted in the Simulations of H-Shaped and A_3AA_3 Polymers

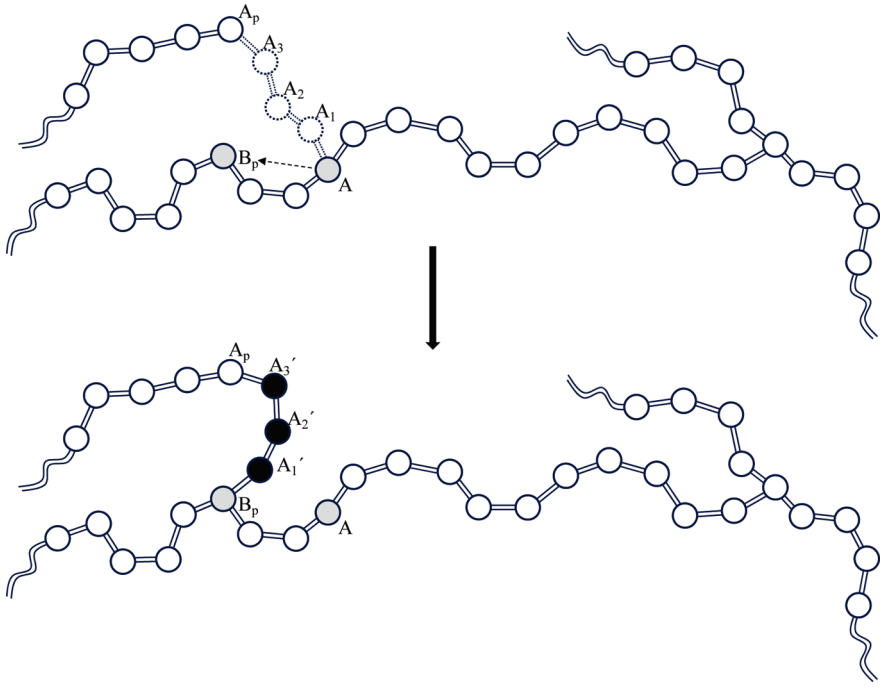

6 carbon atoms long. (We denote this as SCB_48 × 16.5_47 × 6; the first figure represents the number of chain segments or strands along the backbone that are separated by branch points, the second the average number of carbon atoms per chain segment, the third the average number of branches per chain, and the fourth the number of carbon atoms per branch.) All these four systems bear the same number of carbon atoms along their longest chain contour. For the purposes of comparing the properties of different PE architectures also on the basis of the same total chain length, two more systems were selected and simulated: (a) a linear PE melt containing on the average 1072 carbon atoms per chain (denoted as L_1072) and (b) a SCB PE melt containing on the average 512 carbon atoms along the main backbone and 35 short branches, each of which is 8 carbon atoms long. (Following the notation explained above, this is denoted as SCB_36 × 22_35 × 8 and corresponds to an ethylene−1-decene copolymer.) This latter system (although commercially not common) serves the purpose of studying differences in the local or overall conformation of SCB systems having the same total number of carbon atoms but a different number of branches (and thus a different branch length) along their main backbone. A total of 8 chains per simulation cell were used in all cases. The MC simulations were executed in the semigrand statistical ensemble $\{N_{ch}NPT\boldsymbol{\mu}^*\}$[30,31] where the values of the following variables are held fixed: the number of chains N_{ch}, the average number of atoms per chain N, the pressure P, the temperature T, and the spectrum of chain relative chemical potentials $\boldsymbol{\mu}^*$ controlling chain length distributions (since most of the chain connectivity moves employed induce polydispersity).

As has been discussed by Pant and Theodorou[30] for bulk chain systems and by Daoulas et al.[48] for grafted chain systems, polydispersity (i.e., fluctuations) in the chain length distribution in the semigrand ensemble is treated by specifying the spectrum $\boldsymbol{\mu}^*$ of chain relative chemical potentials. An interesting feature of the branched polymers studied here is that one needs to control two different chain length distributions in order to precisely tune their microstructure. This happens because, in addition to the total chain length, the number of carbon atoms between successive branch points can vary in the course of a simulation with the proposed composite algorithm. Alternatively, and instead of the total chain length, one can control the length of the main backbone of the chain. For H-shaped and A_3AA_3 chain systems, there is a third option: one can control the distribution of carbon atoms on the chain crossbar (i.e., on the part of the chain between the two branch points). And this is what we followed in the simulations presented in this work in order to have a precise control on the microstructure of the simulated systems: For the H-shaped and A_3AA_3 polymers, we chose to control separately the distributions of carbon atoms on the chain backbone and the chain crossbar (as a result, the distribution of the total chain length is controlled indirectly); for the SCB systems, on the other hand, we chose to control separately the distributions of the total carbon atoms per chain and of the carbon atoms between two consecutive branch points within a chain. We should also mention here one more method for controlling chain length distribution in SCB polyolefins: It has been followed by Ramos et al.,[40] in their simulations of ethylene−1-hexene copolymers: instead of the distribution of carbon atoms per chain, they steered the distribution of the number of branches in the chain. As we will discuss below, the two methods yield practically identical results.

Once we have decided which chain length distributions to control, the question arises what type of polydispersity to impose and how. To this, we recall that Pant and Theodorou[30] have derived analytical expressions for the spectrum of chain relative chemical potentials that produce the three most common limiting distributions of chain length (or molecular weights): the uniform distribution, the most probable distribution, and the Gaussian distribution. Guided by their analysis and in order to keep the simulation approach as simple as possible, we have decided to make use in this work of the profile of chain relative chemical potentials that for a system of linear chains in the bulk produces a uniform distribution of chain lengths in a prespecified interval around a mean value. More precisely, we chose the width of the uniform distribution to be such that the resulting polydispersity index I is approximately equal to ∼1.083 for all fluctuating molecular lengths in all chain architectures addressed here (linear, H-shaped, A_3AA_3, and SCB). On the basis of the analysis of Pant and Theodorou,[30] if N denotes the number-average molecular length of the distribution in units of CH_2 or CH_3 or

CH groups and Δ its half-width reduced by the number-average chain length N, the value of 1.083 for the polydispersity index I is obtained by choosing $\Delta = 0.5$. This implies that the corresponding chain length distribution is uniform in the interval from $N(1 - \Delta)$ to $N(1 + \Delta)$. As we will check in section 4, the resulting distributions at the end of the MC simulation came out to be (to a very satisfactory degree) indeed uniform in the prespecified intervals for all simulated linear and branched systems. A point worth noting here is that in the present simulations, lengths of odd and even segments in the various chain length distributions are equally probable. This is not the case in real polyolefins where each monomer contributes a pair of backbone atoms because copolymerization catalysts do not have equal probabilities for head-to-head and head-to-tail monomer addition.

Based on the above considerations, for the linear L_792 system, the prespecified interval of allowed chain lengths are (here $N = 792$ and $\Delta = 0.5$) from $792 \times (1 - 0.5)$ to $792 \times (1 + 0.5)$, i.e., the interval [396, 1188]. Similarly, for the L_1072 system (here $N = 1072$ and $\Delta = 0.5$), chain lengths will be allowed to vary uniformly in the interval [536, 1608]. For the H-shaped and A_3AA_3 melts, on the other hand, the intervals of allowed molecular lengths for the chain cross-bar ($N = 512$ and $\Delta = 0.5$) and the four or six branches emanating from it ($N = 140$ and $\Delta = 0.5$) are [256, 768] and [70, 210], respectively. Finally, for the simulated SCB systems, the corresponding intervals of allowed molecular lengths for the total chain ($N = 1072$ or 1074 and $\Delta = 0.5$) and interbranch spacing ($N = 21$ or 15.5 and $\Delta = 0.5$), respectively, are [536, 1608] and [11, 32] for SCB_36 × 22_35 × 8 and [537, 1609] and [8, 24] for SCB_48 × 16.5_47 × 6.

In all simulations, the temperature and pressure were held fixed at $T = 450$ K and $P = 1$ atm, respectively.

In the simulations of the H-shaped and A_3AA_3 structures, the following mix of Monte Carlo moves was employed, which (based on a few trial-and-error runs) was seen to provide practically optimal code performance (see Table 2): X-reptations, 12%; flips, 5% for the H-polymer and 8% for the A_3AA_3 polymer; CONROTs, 20% for the H-polymer and 26% for the A_3AA_3 polymer; d-CONROTs, 4% for the H-polymer and 7% for the A_3AA_3 polymer; DBs, 33% for the H-polymer and 27% for the A_3AA_3 polymer; IDRs, 18% for the H-polymer and 19% for the A_3AA_3 polymer; H-BRs, 7%; volume fluctuations, 1%. In the simulations of the SCB structures, the mix of moves was changed to: reptations, 10%; rotations, 5%; flips, 5%; CONROTs, 20%; d-CONROTs, 19%; EBs, 25%; CCBs, 8%; Br-CCBs, 7%; volume fluctuations, 1%.

4. Results and Discussion

Acceptance Rates of the Employed MC Moves. In Table 2 we report the average acceptance ratios for all MC moves employed in the present simulations with the six different systems (L_792, L_1072, H_512_140, A_512_140, SCB_48 × 16.5_47 × 6, and SCB_36 × 22_35 × 8). In general, the simpler moves (flip, rotation, reptation, and CCB) present acceptance rates that are significantly higher than those of the more advanced ones (EB, DB, IDR, d-CONROT, Br-CCB, and H-BR). But it is through the very drastic changes in chain conformation brought about by these rarely accepted but very efficient moves that the long-length scale features of the studied systems are fully equilibrated within modest CPU time with the new algorithm, provided that the simulation is carried out sufficiently long (see next paragraph). Regarding the dependence of the acceptance ratio on molecular architecture, the data of Table 2 indicate that: (a) Reptation, end-mer rotation, flip, and CONROT are practically insensitive to the linear or nonlinear structure of the PE molecules; the same is true also for the end-bridging (EB), double-bridging (DB), and intramolecular double rebridging (IDR) moves. (b) In contrast, d-CONROT is very sensitive to the type of branched structure it is applied to: its acceptance ratio is very small (although reasonable) in H-shaped and A_3AA_3 PE, but much higher in SCB PE. (c) Volume fluctuations are accepted somewhat faster in branched (e.g., SCB, A_3AA_3, and H-shaped) PE than in linear PE. (d) The effectiveness of CCB and especially of Br-CCB depends critically on the number of interacting sites to be regrown in the course of the move: for example, the acceptance rate of Br-CCB increases from 0.097% in the case of SCB_36 × 22_35 × 8 PE to 0.22% in the case of SCB_48 × 16.5_47 × 6 PE (i.e., more than twice).

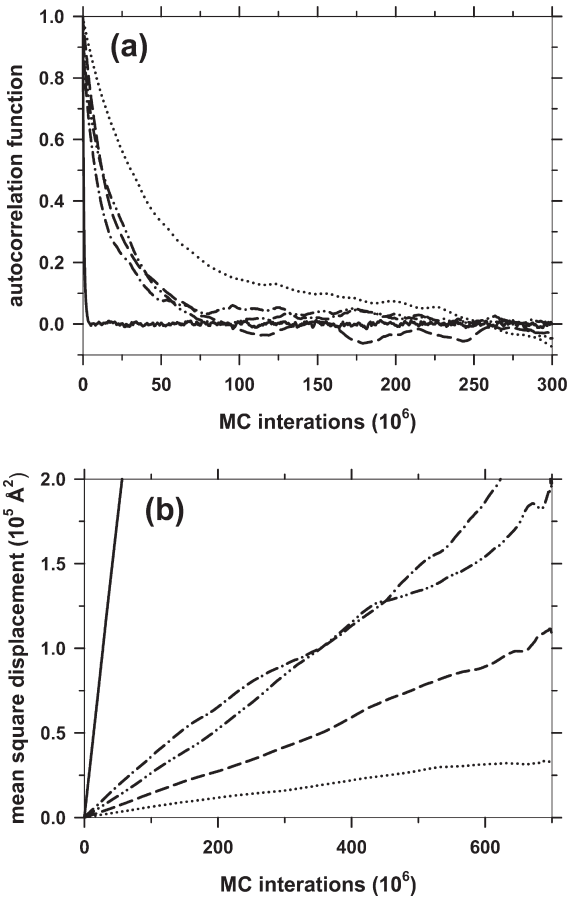

Figure 1. Illustration of the efficiency of the Monte Carlo algorithm for simulating H-shaped, A_3AA_3, and SCB polymers, in terms of (a) the decay of the autocorrelation function $\langle \mathbf{u}(t) \cdot \mathbf{u}(0) \rangle$ of the unit end-to-end vector of chain backbone $\mathbf{u}(t)$ and (b) the mean-square displacement $\langle (\mathbf{R}_G(t) - \mathbf{R}_G(0))^2 \rangle$ of the chain center-of-mass position $\mathbf{R}_G(t)$, with computational time. The L_1072, H_512_140, A_512_140, SCB_36 × 22_35 × 8, and SCB_48 × 16.5_47 × 6 systems are represented by the solid, dashed, dotted, dash-dot, and dash-dot-dot lines, respectively. All simulations were conducted at $T = 450$ K and $P = 1$ atm.

Algorithm Efficiency. To assess the efficiency of the new MC algorithm, we have examined the rate of decay of the autocorrelation function of the unit chain end-to-end vector $\langle \mathbf{u}(t) \cdot \mathbf{u}(0) \rangle$ and the rate of the mean-square displacement (msd) of the chain center-of-mass $\langle (\mathbf{R}_G(t) - \mathbf{R}_G(0))^2 \rangle$ as a function of the number of MC iterations attempted. The results obtained for the six simulated systems (L_792, L_1072, H_512_140, A_512_140, SCB_48 × 16.5_47 × 6, and SCB_36 × 22_35 × 8) are presented in Figure 1. Figure 1a, in particular, shows that for all systems $\langle \mathbf{u}(t) \cdot \mathbf{u}(0) \rangle$ drops eventually to zero, indicative of a fully relaxed polymer configuration. In particular, it takes about 10^7 MC iterations

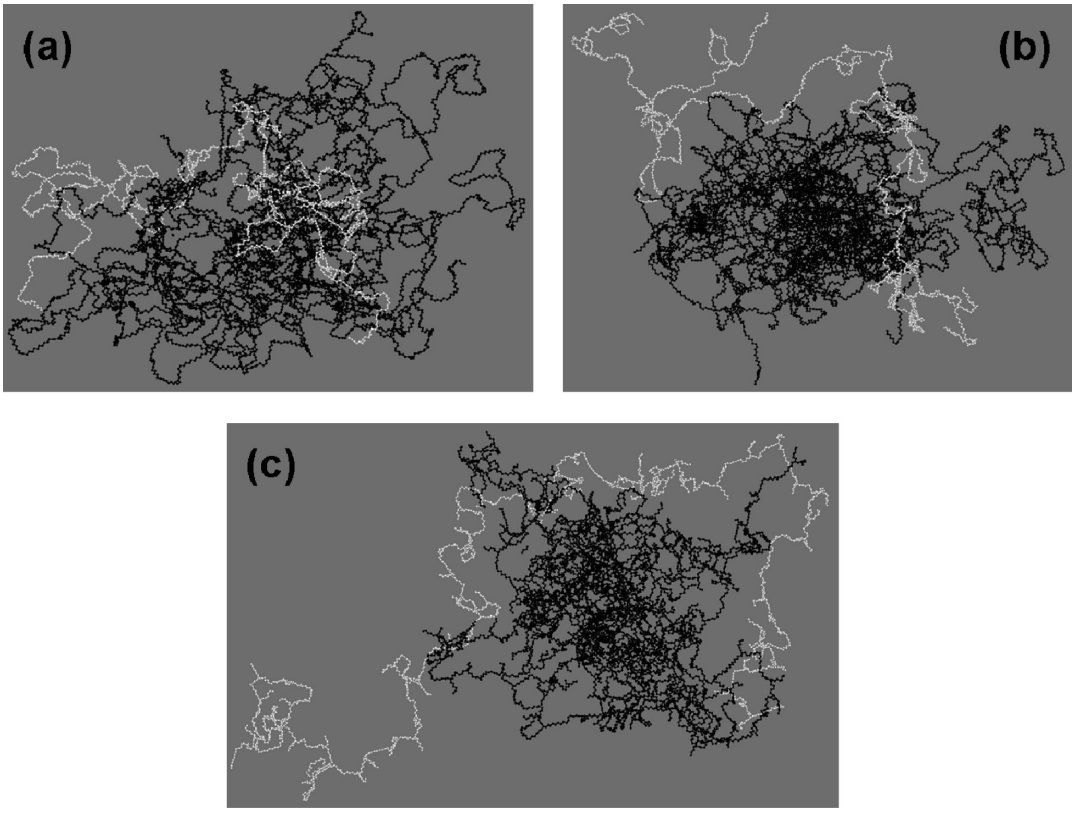

Figure 2. Representative atomistic snapshot from the fully equilibrated part of the trajectory accumulated in the course of the present MC simulations for (a) the H_512_140, (b) the A_512_140, and (c) the SCB_48 × 16.5_47 × 6 PE system. Shown in bright white color is a single chain out of the eight present in the simulation box. All simulations were conducted at $T = 450$ K and $P = 1$ atm.

for $\langle \mathbf{u}(t) \cdot \mathbf{u}(0) \rangle$ to drop to zero in the case of the linear systems, about 9×10^7 in the case of the SCB and H-shaped ones, and about 2.5×10^8 in the case of the $A_3\mathbf{A}A_3$ polymer. Clearly, the $A_3\mathbf{A}A_3$ system is the most difficult to equilibrate; it is very promising, however, that even for this system the total real time needed for $\langle \mathbf{u}(t) \cdot \mathbf{u}(0) \rangle$ to drop to zero is less than 1 week (we report that on an Intel Dual Core 3 GHz CPU, it takes ~6 days each of the simulated systems to complete 10^8 MC iterations). For comparison, we mention that the longest (end-to-end) relaxation time of A_512_140 PE (the most demanding computationally) is estimated to be on the order of 10 μs. Given that even on the fastest CPU available today one can track up to 5 ns of real time per day with MD, we conclude that we would have to wait for several years(!) (even with the most efficient parallelization techniques available and code execution on several CPUs) for $\langle \mathbf{u}(t) \cdot \mathbf{u}(0) \rangle$ to drop to zero. This is considered as the biggest advantage of the designed MC algorithm over any dynamic method, which (by nature) are applicable today to considerably shorter-chain systems. The same conclusion is drawn if we look at the plots of the chain center-of-mass msd versus number of MC iterations attempted. Focusing, in particular, on A_512_140 PE, we see that after 2×10^8 MC iterations $\langle (\mathbf{R}_G(t) - \mathbf{R}_G(0))^2 \rangle$ has traveled a distance of $\sim 1.2 \times 10^4$ Å^2; as we will see below, this corresponds to ~3 times its mean-square radius of gyration.

Typical atomistic snapshots of fully equilibrated system configurations at the end of the simulation with the new MC algorithm for the H_512_140, A_512_140, and SCB_48 × 16.5_47 × 6 PE systems are shown in Figure 2. The bright white color depicts the instantaneous conformation of just one of the chains (out of the eight) present in the simulation cell.

Table 3. Characteristic Chain Dimensions of the Linear and Branched Polyethylene Melts Simulated at $T = 450$ K and $P = 1$ atm

system	ρ (g/cm^3)	$\langle R^2(N) \rangle / N l_{eq}^2$ [a]	$\langle R_g^2(N) \rangle / N l_{eq}^2$	l_p (Å)[b]
Linear_792	0.774 ± 0.002	9.25	1.52	8.2
Linear_1072	0.777 ± 0.002	9.31	1.54	8.4
H_512_140	0.777 ± 0.003	9.92 (9.94)	1.35	9.3
A_512_140	0.781 ± 0.004	11.8 (11.1)	1.30	9.6
SCB_36 × 22_35 × 8	0.776 ± 0.005	9.26	1.09	11.2
SCB_48 × 16.5_47 × 6	0.782 ± 0.004	8.72	1.11	11.6

[a] Two values are reported for the H_512_140 and A_512_140 PE systems: one based on the chain backbone (containing 512 carbon atoms on average) and another (shown in parentheses) based on the longest linear dimension (containing 792 carbon atoms on average). [b] Computed according to eq 5.

Density. Table 3 shows the results of the present $\{N_{ch}NPT\mu^*\}$ MC simulations for the density of the six simulated PE melts. We see that within the statistical uncertainty all of them (linear, H-shaped, $A_3\mathbf{A}A_3$, and SCB ones) are characterized by a similar density (approximately equal to 0.777 g/cm^3). The maximum difference is recorded between the L_792 and the SCB_48 × 16.5_47 × 6 systems and is on the order of 0.008 g/cm^3. The corresponding experimental values are about 0.767 g/cm^3 for linear PE and about 0.768 g/cm^3 for SCB PE systems.[40] The simulation data (although slightly overestimating the experimental densities) are therefore in support of a rather negligible effect of chain branching on density (and the rest of the volumetric properties) of polyethylene, which agrees with the actual experimental measurements. Experimentally, it is believed that the use of α-olefins longer than propylene enhances somewhat the reduction of density at a given mole fraction.[6]

Chain Dimensions. Figure 3 shows plots of the running average values of the mean-square end-to-end distance $\langle R^2 \rangle$

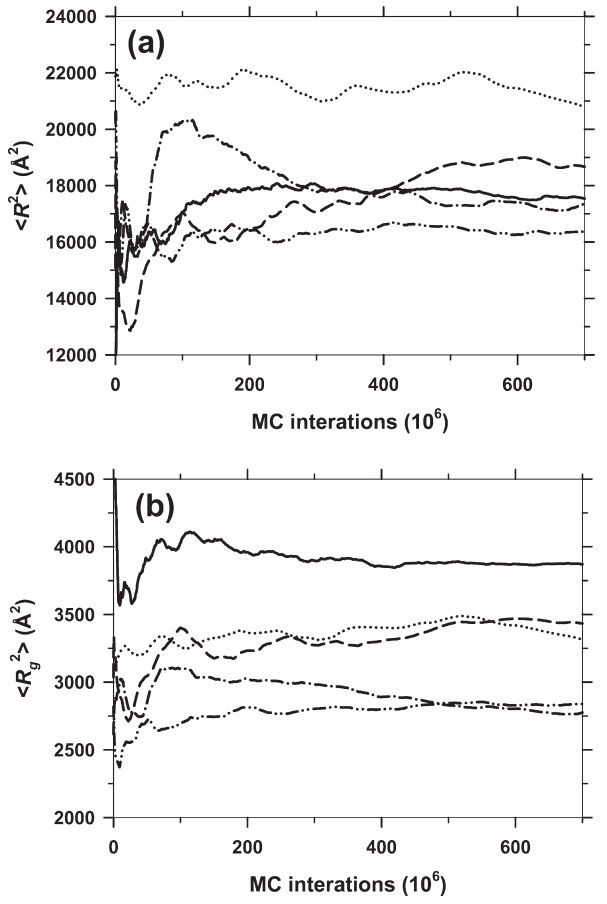

Figure 3. Comparing the dimensions of branched polymers (H_512_140, dashed lines; A_512_140, dotted lines; SCB_36 × 22_35 × 8, dash-dot lines; SCB_48 × 16.5_47 × 6, dash-dot-dot lines) with those of the corresponding linear analogue (solid lines). Results for (a) the mean-square end-to-end distance $\langle R^2 \rangle$ of the longest linear chain dimension and (b) the mean-square radius of gyration $\langle R_g^2 \rangle$. The reference linear system is L_792 in (a) (i.e., the linear with the same number of carbon atoms along the longest linear dimension of the branched polymers) and L_1072 in (b) (i.e., the linear with the same total number of carbon atoms). Furthermore, in (b) the $\langle R_g^2 \rangle$ values for the A_512_140 PE system have been rescaled by the factor 1352/1072 (= 1.26).

referring to the longest chain dimension along its contour and of the mean-square chain radius of gyration $\langle R_g^2 \rangle$ for all simulated PE melts. The large end-to-end distance fluctuations recorded in the figure are indicative of the efficiency with which the designed composite MC algorithm samples phase space. Predicted $\langle R^2 \rangle$ and $\langle R_g^2 \rangle$ values for all simulated systems are reported in Table 3. For the H_512_140 and A_512_140 melts, in particular, two different $\langle R^2 \rangle$ values are reported in Table 3: one based on the chain crossbar (containing 512 carbon atoms on average) and another based on the longest linear dimension of the system (containing 792 carbon atoms on average). On the basis of the data of Table 3, the H-shaped and A_3AA_3 polymers are seen to exhibit significantly higher $\langle R^2 \rangle$ values than the corresponding linear analogue with the same number of carbon atoms along the backbone (L_792), implying an extension of their main backbone; this is more pronounced for the A_512_140 system. It seems that the long branches that emanate from the two ends of the main crossbar exert an entropic, tensile force on the backbone, causing an increase in its dimension compared to that of the linear analogue with free ends. This observation is in agreement with the proposed pom-pom model[13] for H-shaped and A_3AA_3 polymers, according to which a stretching force is exerted by each dangling arm on chain backbone, equal to $f = 3k_BT/a$ where a is the tube diameter representing topological interactions. In contrast, the SCB_48 × 16.5_47 × 6 and SCB_36 × 22_35 × 8 PE systems are characterized by $\langle R^2 \rangle$ values that are shorter than those of the linear analogue (L_792), implying a more compact chain conformation for these polymers. This becomes more evident as the branch length is decreased and the number of branches per chain increases (keeping the backbone length constant).

A more representative measure of the chain dimensions of the linear and branched PE architectures studied is offered by the mean-square chain radius of gyration $\langle R_g^2 \rangle$. The data reported in Table 3 and the plots presented in Figure 3b suggest that all branched systems are characterized by $\langle R_g^2 \rangle$ values which are smaller than that of their linear analogue of the same total chain length (L_1072), indicating a more compact arrangement of the carbon atoms around their chain center-of-mass. In fact, the $\langle R_g^2 \rangle$ data demonstrate that the most compact chain arrangement is exhibited by the SCB polymers, which is absolutely consistent with the information provided by the $\langle R^2 \rangle$ results.

As discussed by Ramos et al.,[40] simulation predictions for the mean-square radius of gyration $\langle R_g^2 \rangle$ for SCB systems can be directly compared against actual experimental data from small-angle neutron scattering (SANS) measurements by plotting the ratio $\langle R_g^2 \rangle / M$ (where M is the total molecular weight of the polymer) as a function of the average molecular weight per backbone bond, m_b. The results obtained for the two SCB PE systems simulated here (SCB_48 × 16.5_47 × 6 and SCB_36 × 22_35 × 8 with m_b = 18.9 g/mol) are 1.89 and 1.85 nm^2 mol kg^{-1}, respectively. The corresponding experimental value for ethylene−1-butene copolymers with m_b = 18.9 g/mol (corresponding to two methylene units per branch) is 1.52 nm^2 mol kg^{-1}.[49,50]

Qualitatively, our conclusions from the present simulation studies for the role of branch content (and degree of branching) on the conformational stiffness of branched polymers are consistent with those drawn from theoretical calculations, other simulation studies, and/or experimental measurements.[51−53] As far as a quantitative comparison with these earlier works for the overall dimensions of the simulated systems is concerned, we report that our simulation results for the ratio $g \equiv \langle R_g^2 \rangle_{branched} / \langle R_g^2 \rangle_{linear}$ of the mean-square radii of gyration of branched and linear PE molecules of the same total number of carbon atoms come out to be equal to 0.877, 0.844, 0.721, and 0.708 for the H_512_140, A_512_140, SCB_48 × 16.5_47 × 6, and SCB_36 × 22_35 × 8 melts, respectively. These values are somewhat larger than theoretical predictions based on the Gaussian chain model[51] and simulation and experimental data[52,53] which suggest g values between 0.69 and 0.72 for H-shaped polymer chains in solution, almost independent of the solvent quality.

Packing Length. The packing length is an important measure of chain structure, since it is linked with its rheological behavior (i.e., its response to an applied flow field).[49,50] It is defined as the ratio between the apparent volume per molecule in the system and the effective chain dimension; it takes therefore smaller and smaller values as the effective space occupied by a chain increases. As discussed by Lohse,[50] if we use the mean-square chain end-to-end distance to quantify chain dimensions, then the packing length is denoted by p and is mathematically defined as

$$p = \frac{V_{occ}}{\langle R^2 \rangle} \tag{4}$$

If, on the other hand, the mean-square chain radius-of-gyration is chosen to quantify chain dimensions, then the packing length is denoted by l_p and is mathematically defined as

$$l_p = \frac{V_{occ}}{\langle R_g^2 \rangle} \quad (5)$$

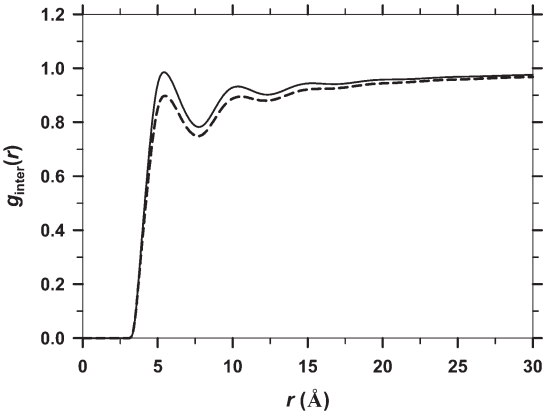

Figure 4. Intermolecular mer−mer pair distribution function $g_{inter}(r)$ for the linear, H-shaped, and A_3AA_3 systems (solid line) and the two SCB polyolefins (dashed line). As explained in the main text, we show only two curves because the first group of systems (L_1072, H_512_140, and A_512_140) gave identical curves (computed $g_{inter}(r)$ curves were practically indistinguishable from each other for all of them), and the same was true for the second group (SCB_48 × 16.5_47 × 6 and SCB_36 × 22_35 × 8).

Ramos et al.[40] have analyzed in detail the dependence of the packing length l_p for ethylene−1-hexene copolymers and have found that to a very good approximation

$$l_p\ (\text{Å}) = 0.27 m_b^{1.34} \quad (\text{simulation}, T = 450\ \text{K}) \quad (6)$$

This agrees very well with experimental data which are in favor of the following relationship between l_p and m_b:

$$l_p\ (\text{Å}) = 0.33 m_b^{1.29} \quad (\text{experiment}, T = 463\ \text{K}) \quad (7)$$

The results obtained for the two SCB melts discussed here using eq 5 in the form

$$l_p = \frac{M}{\rho N_A \langle R_g^2 \rangle} \quad (8)$$

where M is the chain molecular weight and N_A Avogadro's number, are l_p = 11.6 Å for SCB_48 × 16.5_47 × 6 PE and 11.2 Å for SCB_36 × 22_35 × 8 PE; these are slightly more consistent with eq 6 than with eq 7. We further note that for the L_1072 PE system the present MC simulations predict an l_p value equal to 8.4 Å. The predictions of our MC simulations for the packing length of all six PE systems simulated here are reported in the last column of Table 3. We see that at the conditions of the simulation (T = 450 K and P = 1 atm), the H-shaped and A_3AA_3 PE systems are characterized by l_p values that are approximately 10−20% higher than that of strictly linear PE, while the two SCB PE systems exhibit even higher (up to 40%) l_p values. These results compare very favorably with the measurements of

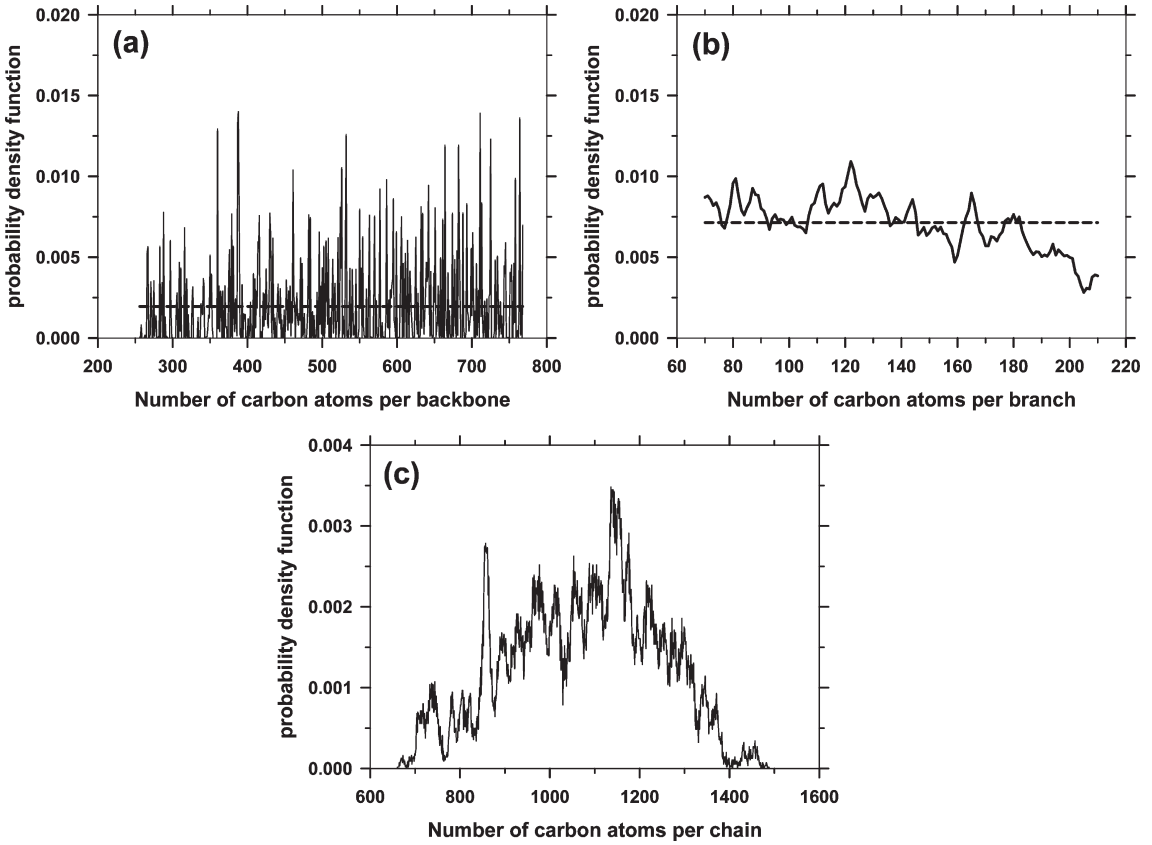

Figure 5. Chain length distributions of carbon atoms along (a) the main-chain backbone, (b) the chain crossbar (interbranch spacing), and (c) the entire chain for the H_512_140 PE system. The theoretically expected distributions in (a) and (b) are the uniform ones in the intervals [256, 768] and [70, 210], respectively, corresponding to a polydispersity index I = 1.083; it is shown by the dashed lines in the figure.

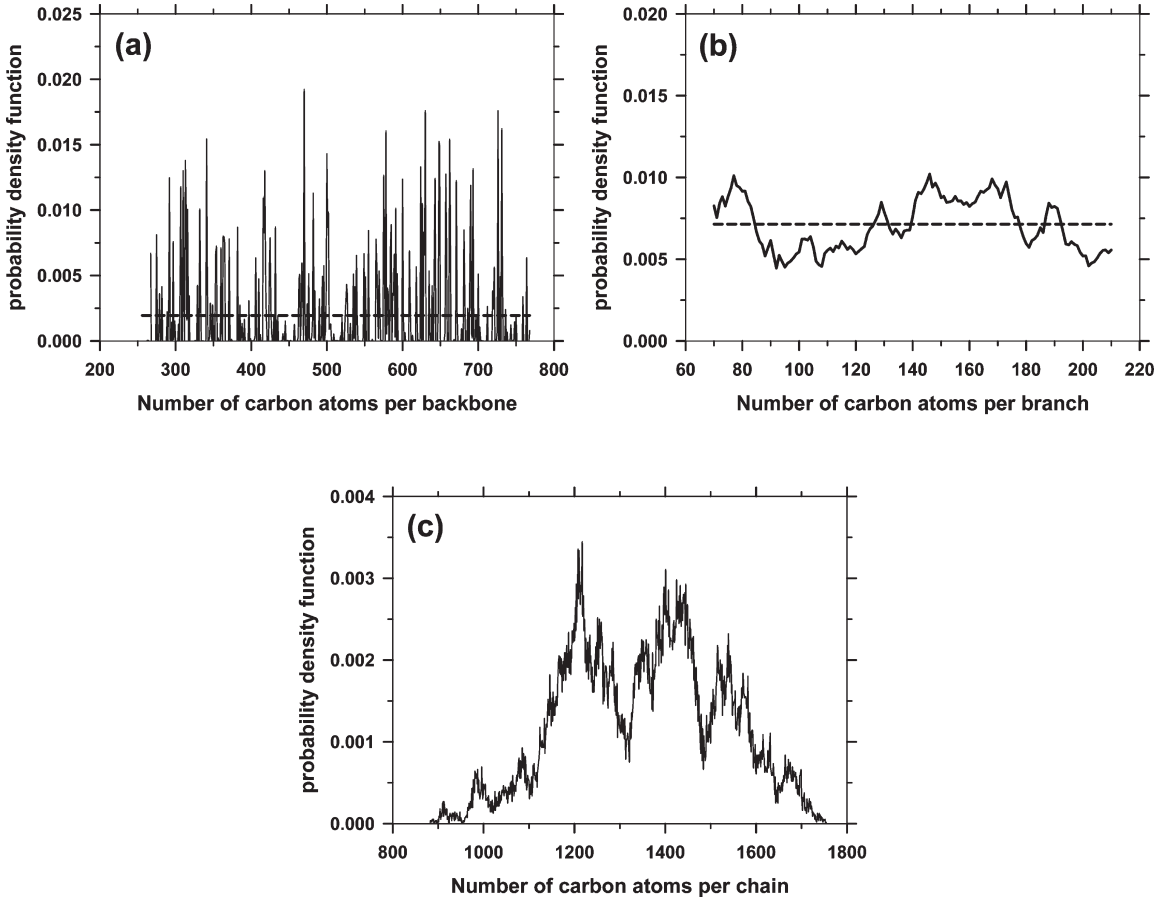

Figure 6. Same as with Figure 5, but for the A_512_140 PE system.

Ramachandran et al.[54] based on small-angle neutron scattering data according to which the value of l_p ranges from 6.5 ± 0.8 Å for linear polyethylene to 9.0 ± 0.6 Å for polyethylene with 12.1 branches per 1000 carbon atoms. Ramachandran et al.[54] have further suggested a relationship between number of SCBs and l_p, which indicates a maximum enhancement of persistence length to 9.1 Å for fully branched PE (i.e., when all carbon atoms in the backbone are branched).

Intermolecular Radial Pair Distribution Function. More insight into the structural properties of the simulated PE systems can be gained by computing the intermolecular radial pair distribution function, $g_{inter}(r)$, and analyzing how it varies from system to system. The results obtained are shown in Figure 4. Linear, H-shaped, and A_3AA_3 systems are found to be characterized by the same $g_{inter}(r)$ curves, and the same was observed for the two SCB melts. Thus, only two sets of data are reported in Figure 4: the first (depicted by the solid line) corresponds to all linear, H-shaped, and A_3AA_3 melts and the second (depicted by the dashed line) to the two SCB poyolefins. Our results show that the first peak in the $g_{inter}(r)$ curves of the SCB melts is significantly smaller than that for the rest of the melts; its position is also seen to be shifted slightly to the right. In general, the entire $g_{inter}(r)$ curve for the SCB systems is always below the curve corresponding to the linear, H-shaped, and A_3AA_3 melts, implying a somewhat stronger correlation hole effect for this category of systems. The two sets of curves (the one corresponding to the linear, H-shaped, and A_3AA_3 melts and the other corresponding to the SCB ones) converge to each other only for radial distances longer than about 30 Å.

Total and Interbranch Chain Length Distributions. In order to see whether the imposed MC criteria have been correctly realized in the simulation, we have investigated the resulting probability distribution of backbone, branch, and total chain lengths. In Figure 5 we present the result for the H_512_140 system where we imposed uniform molecular weight distributions separately (i.e., independently) for the chain backbone and the chain branches (or, equivalently, the chain crossbar). The curves reported in Figure 5a,b show that the uniformity of both distributions is satisfied within the statistical uncertainty. Furthermore, given the two (statistically independent) uniform distributions, their sum (defining the total chain length) is to follow a Gaussian-type distribution, which is indeed the case observed in the simulations (see Figure 5c). The same molecular weight criteria for the backbone and chain branches (or, equivalently, the chain crossbar) have been applied in the simulations with the A_512_140 PE system, and a similarly satisfactory result is observed in Figure 6 (with larger statistical fluctuations). In the case of SCB polymers, different criteria for the molecular weight distributions were used; here we imposed a uniform distribution for the total chain length and the branch-to-branch frequency (see Figure 7). The data reported in parts b and d of Figure 7, in particular, confirm that the two distributions are correctly realized at the end of the MC simulation.

Bond Angle and Torsion Angle Distributions. The distributions of bond-bending and torsional (dihedral) angles for the simulated branched PE systems are shown in Figures 8 and 9. Guided by the different values of the parameter sets governing the corresponding potential functions, two different sets of distributions are shown in each figure: the first refers to

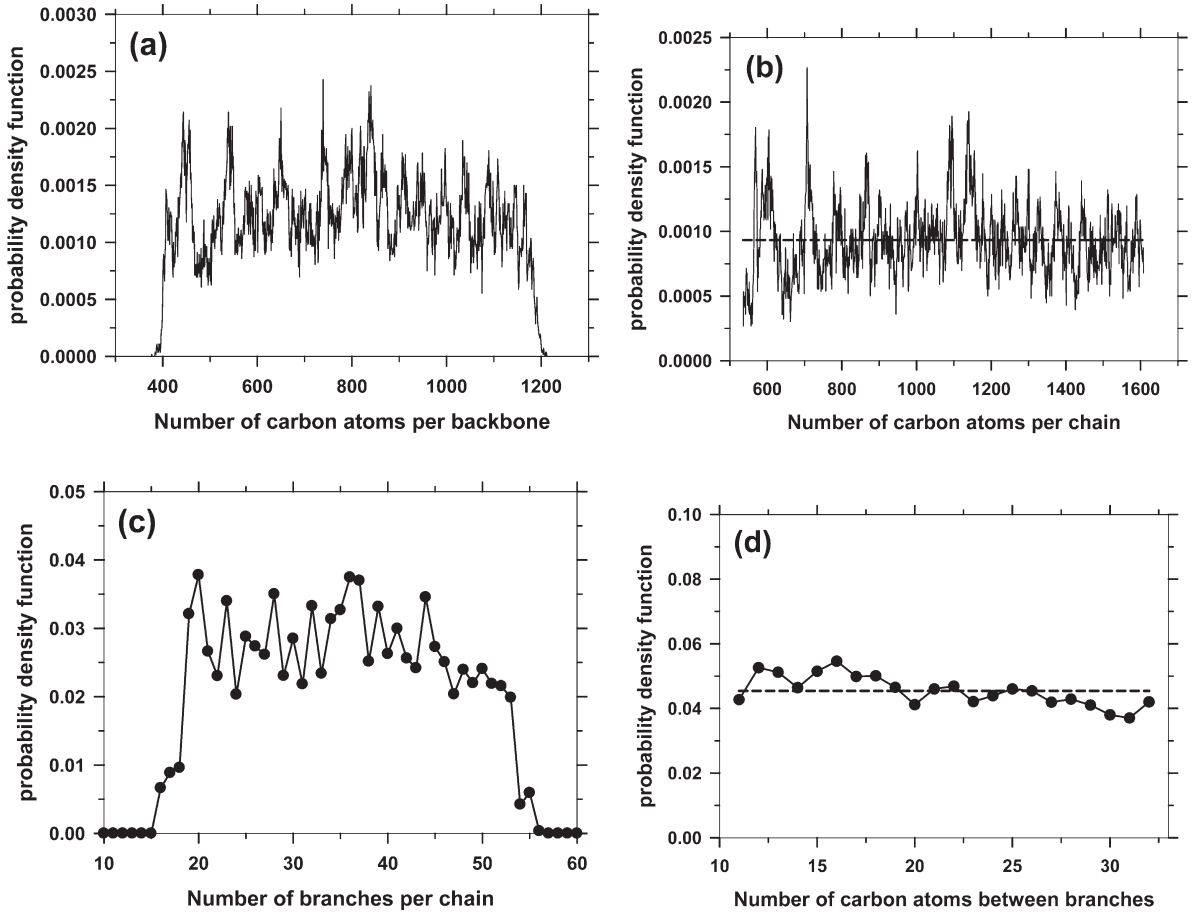

Figure 7. (a) Chain length distribution of carbon atoms along the main chain backbone. (b) Chain length distribution of carbon atoms along the entire chain. (c) Distribution of the number of branches per molecule. (d) Distribution of the number of carbon atoms between two successive branches. All results refer to the SCB_36 × 22_35 × 8 PE melt at T = 450 K and P = 1 atm. The theoretically expected distributions for the total and branch-to-branch lengths are the uniform ones in the intervals [536, 1608] and [11, 32], respectively, corresponding to a polydispersity index I = 1.083; they are shown by the dashed lines in the figure.

backbone angles and the second to branch angles. Furthermore, since we found that the distribution of both types of angles for backbone atoms was the same for all systems irrespective of their molecular architecture (linear, H-shaped, A_3AA_3, and SCB ones), only one curve is shown for all backbone angles in part a of the two figures. We observe that the curves have in all cases shapes that very much resemble those expected from the well-known Boltzmann distribution for the potential energy functions given in Table 1. This is especially true for the bond angles. For the torsional angles, a closer inspection of the curves reported in Figure 9a,b reveals that the atoms near branch points are characterized by a significantly smaller relative population of *trans* conformations than atoms far away from them. This is displayed in Figure 9b for the SCB_48 × 16.5_47 × 6, but it is true also for the branch torsion angles in the other systems. By comparing, in fact, the distribution of branch torsion angles in the two different SCB melts (SCB_48 × 16.5_47 × 6 and SCB_36 × 22_35 × 8), we see that this does not depend critically on branch length or branch frequency.

We further computed the mean square end-to-end distance of branches in the SCB_48 × 16.5_47 × 6 and SCB_36 × 22_35 × 8 systems and found them to be equal to 45.3 and 70.8 Å^2, respectively. Comparing then with the corresponding dimensions of linear segments of the same length indicates that branches in these SCB melts assume rather stiff conformations, especially in the SCB_48 × 16.5_47 × 6 system. This conclusion is supported by additional computations of the local branch orientation with respect to the main-chain backbone. We found that, on the average, branches tend to emanate from the backbone in directions that form angles ranging from 60° to 90° relative to the local chain direction. The main conclusion to be drawn from all this information is that branches in SCB systems exhibit rather extended configurations (due to steric hindrance effects), which are more pronounced for the shorter ones (i.e., the shorter the branch the higher its conformational stiffness).

Intrinsic Molecular Shape. According to the pioneering work of Šolc and Stockmayer,[55] the intrinsic shape of random walk chains at equilibrium in the eigenvector space of the instantaneous radius of gyration tensor is far more like a "cake of soap" than like a spherical or ellipsoidal one of approximately Gaussian form. Theodorou and Suter[56] have verified this by analyzing a large number of conformations of unperturbed polypropylene chains with Monte Carlo using a rotational isomeric state model. Mavrantzas and Theodorou,[57] on the other hand, have reported that under the application of a strong enough elongational field short PE chains (e.g., C_{24}) are partially unraveled to intrinsically more elongated shapes; thus, instead of a cake of soap, the segment cloud takes an elongated, cigarlike shape. Guided by these studies, in Figure 10 we present additional results revealing the intrinsic shape of the highly branched molecular architectures simulated in this work. The figure shows the segment cloud (i.e., the density distribution of segments around the chain center-of-mass) as computed in the space of

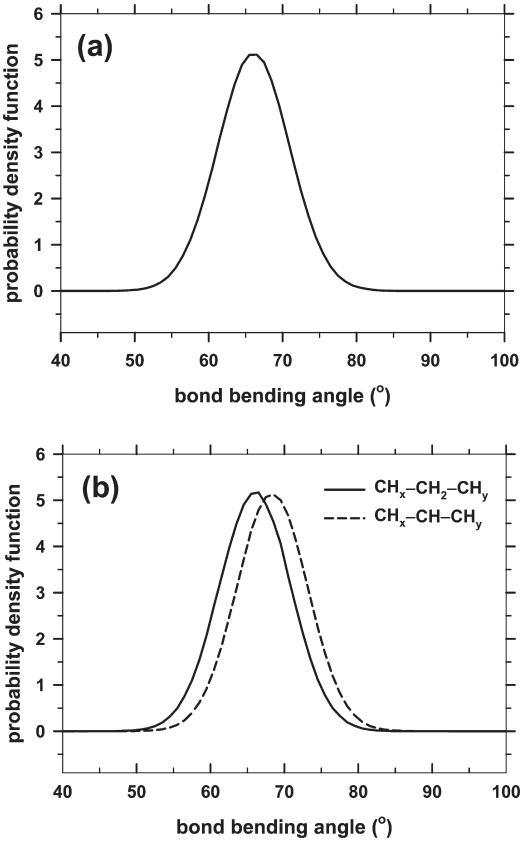

Figure 8. (a) Probability distribution function of the backbone bond angles in the six simulated systems (since practically identical results were obtained for all of them, only one curve is shown). (b) Probability distribution function of the two branch bond angles CH_x–CH_2–CH_y and CH_x–CH–CH_y in the two SCB systems. In all cases, $T = 450$ K and $P = 1$ atm.

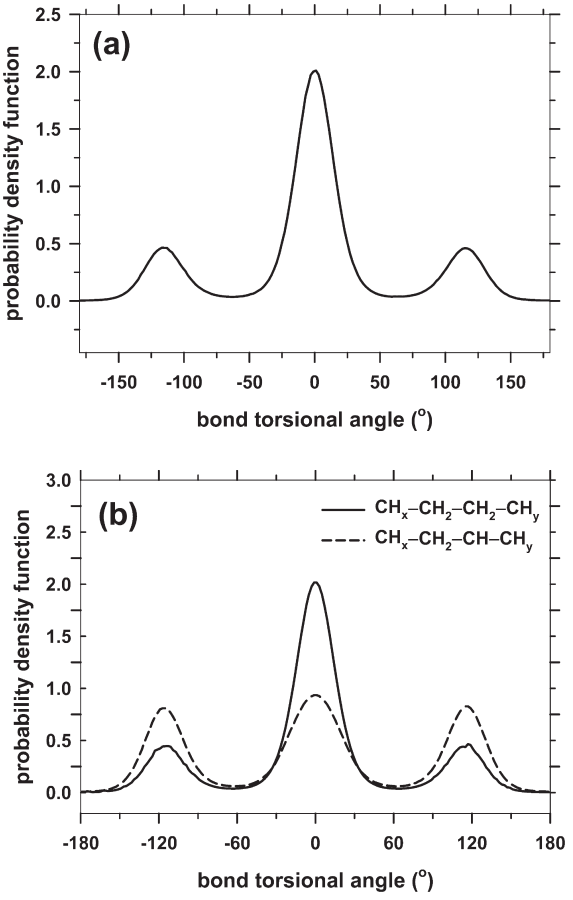

Figure 9. (a) Probability distribution function of the backbone torsion angles in the six simulated systems (since practically identical results were obtained for all of them, only one curve is shown). (b) Probability distribution function of the two branch torsion angles CH_x–CH_2–CH_2–CH_y and CH_x–CH_2–CH–CH_y in the two SCB systems. In all cases, $T = 450$ K and $P = 1$ atm.

eigenvectors of the instantaneous radius of gyration tensor,[55,56] for various values of the monomer density. For all systems, the resulting shapes are consistent with those expected for random walks: they resemble a "cake of soap" instead of having a spherical or ellipsoidal shape.[55] However, as the segment density increases (from the bottom to the top in Figure 10), we observe significant differences in the shapes of the different polymer architectures. Compared, for example, to the linear analogue of the same total chain length (L_1072), the characteristic thin stem or neck exhibited at intermediate values of the segment density is more pronounced in the H_512_140 PE melt, implying a higher number of segments near branch points than deeper along the crossbar. This is even more pronounced in the case of the A_512_140 polymer, for which the number of arms emanating from each of its branch points is 3 (compared to 2 in H-polymers). [A similar behavior has been observed very recently in a nonequilibrium molecular dynamics study[58] of a short H-shaped polymer melt (containing 78 carbon atoms in the crossbar and 25 carbon atoms in each one of its four branches) under flow conditions. For the case of planar elongation, in particular, and for low-to-intermediate values of the cloud density, the H_78_25 melt was seen to exhibit a characteristic arrangement wherein the two dense cores of highest density are connected with a thin and rather uniform stem, a shape which resembles that of a *dumbbell*; in contrast, the molecular shape of the linear analogue subjected to the same type and strength of flow was seen to be more *needlelike*.] The SCB systems, on the other hand, exhibit a flatter and more uniform segment distribution: the characteristic thin neck in these systems is considerably less pronounced. All these observations are consistent with the results presented in Figure 3 for the dependence of $\langle R^2 \rangle$ and $\langle R_g^2 \rangle$ on the microstructure of the simulated systems and the conclusions drawn there about the different conformational stiffness characterizing these systems. From a theoretical point of view, the plots of the segment clouds reported in Figure 10 (and additional ones published in ref 58) may have important implications for methods that employ mechanical or approximate molecular models, such as the FENE dumbbell, the soft (and supersoft) particle, and the pom-pom ones, for studying the flow behavior of polymers as a function of their molecular architecture: these models should be designed in such a way that their response to an applied flow field is consistent with the picture that emerges from the direct atomistic simulation studies.

5. Conclusions and Future Plans

Our goal in this work has been twofold: (a) to provide extensions of newly developed chain connectivity altering MC moves for polymer architectures more complicated than linear and (b) to demonstrate that by integrating them in a composite algorithm, a powerful MC method can be designed capable of simulating branched polymers with a wide variety of chain architectures. We have been able, in particular, to equilibrate and simulate branched PE systems with very long chains, which is almost impossible today by MD. We have succeeded in this by

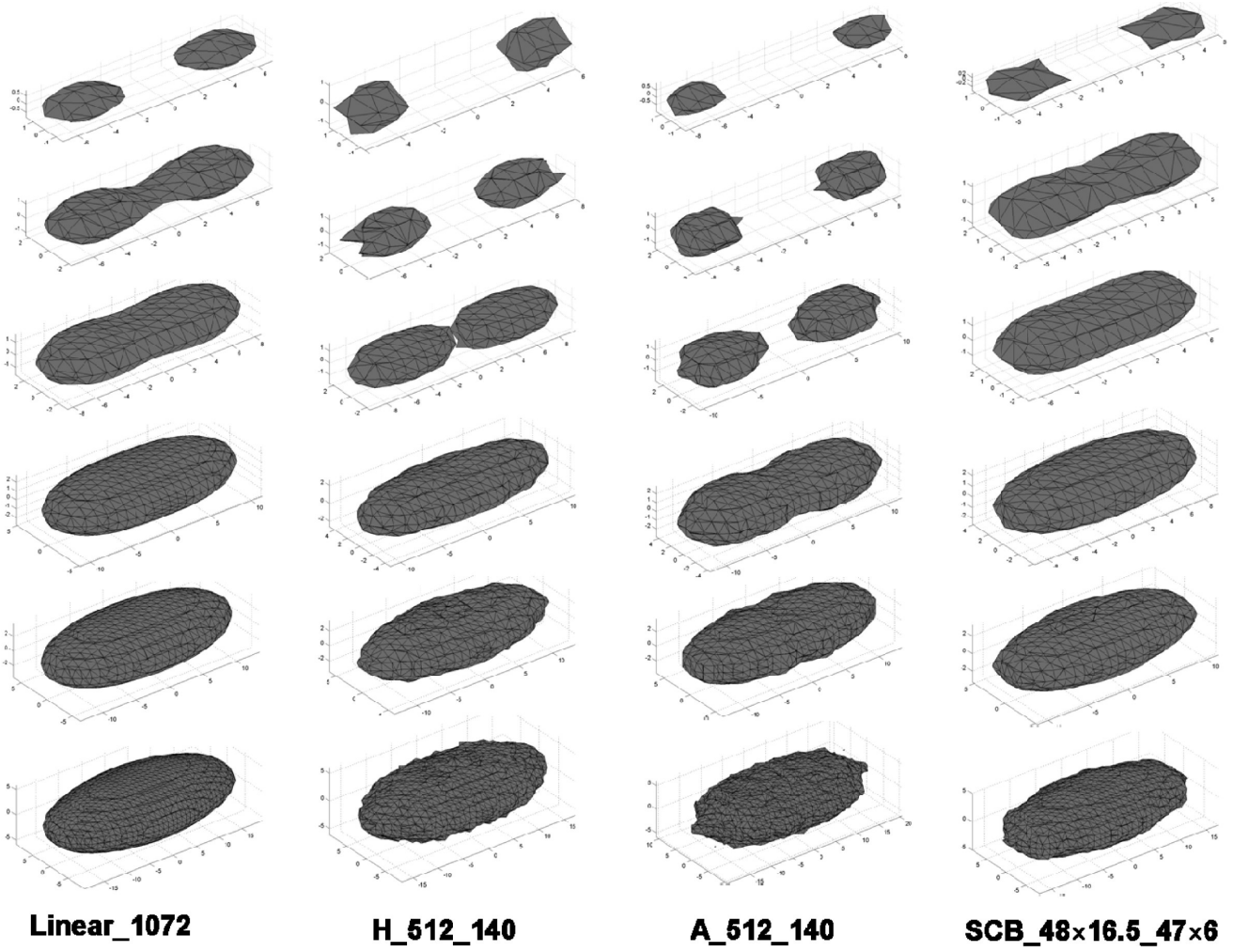

Figure 10. Intrinsic molecular shapes in the L_1072, H_512_140, A_512_140, and SCB_48 × 16.5_47 × 6 PE systems and their comparison based on isosurface plots computed at equal values of the (number-averaged) monomer (or segment) number density in the frame of the principal axes (corresponding to the three eigenvectors) of the instantaneous radius of gyration tensor. For each system, the pictures from the bottom to the top represent the molecular shapes that include 95, 70, 50, 20, 10, and 5% of the total number of segments, respectively.

supplementing classical MC moves such as reptation, X-reptation, flip, CONROT, and CCB with more advanced ones such as d-CONROT, Br-CCB, DB, IDR, and H-Br. Br-CCB, in particular, which has been implemented in the simulations with SCB polyolefins, is suitable for relaxing local segmental motions in the vicinity of the branch points and along the branches, by allowing branch points to move back and forth along the backbone and by regrowing branches in an energetically biased fashion.

Overall, our MC data for the chain dimensions and the packing length of the simulated systems reveal that SCB polyolefins are characterized by a stiffer conformation and a more compact structure than H-shaped and A_3AA_3 systems of the same total chain length, which, in turn, appear to be stiffer than their corresponding linear analogues.

The design of the new composite MC algorithm has been contrived with the following two aims in mind regarding future efforts: first to enable a molecular-level study of the static properties of branched polymers as a function of their molecular architecture (e.g., branch length and branch density) and second to obtain well-equilibrated configurations of model branched systems which could be then amenable to a direct topological analysis aiming at determining the entanglement network underlying their structure at the nanoscale. This is at the heart of modern tube models and theories for understanding and explaining the origin of the unique (and sometimes truly extraordinary) rheological properties exhibited by branched polymers. Work is currently in progress in this direction along with efforts to reformulate the variety of possible MC moves presented here for other realistic polymer architectures such as dendrimers,[59] stars,[60] and hyperbranched molecules.[61]

Acknowledgment. The help of Mr. Vasilis Dimitriadis and Dr. Nikos Karayiannis in the initial phase of this work, in particular their contribution to translating part of the Monte Carlo algorithm presented here into a set of Fortran subroutines, is greatly acknowledged. We are deeply indebted to Dow Benelux B.V. (especially to Dr. Joey Storer, Dr. Jaap den Doelder, and Dr. Rudy Koopmans) for financial support, their genuine interest in the development of new Monte Carlo algorithms for branched PE systems, and above all the many interesting and fruitful discussions we have had with them in the course of this work.

References and Notes

(1) Voit, B. I.; Lederer, A. *Chem. Rev.* **2009**, DOI: 10.1021/cr900068q.
(2) Takur, N. M.; Sharkh, B. F. A.; Osei-Twton, E. Y.; Hussein, I. A. *Macromol. Symp.* **2008**, *263*, 121.
(3) Kapnistos, M.; Lang, M.; Vlassopoulos, D.; Pyckhout-Hintzen, W.; Richer, D.; Cho, D.; Chang, T.; Rubinstein, M. *Nat. Mater.* **2008**, *7*, 997.
(4) Watanabe, H.; Matsumiya, Y.; van Ruymbeke, E.; Vlassopoulos, D.; Hadjichristidis, N. *Macromolecules* **2008**, *41*, 6110.

(5) Connal, L. A.; Vestberg, R.; Hawker, C. J.; Qiao, G. G. *Macromolecules* **2007**, *40*, 7855.
(6) Dealy, J. M.; Larson, R. G. *Structure and Rheology of Molten Polymers: From Structure to Flow Behavior and Back Again*: Hanser Gardner Publications: Cincinnati, OH, 2006.
(7) Kudo, H.; Makino, S.; Kameyama, A.; Nishikubo, T. *Macromolecules* **2005**, *38*, 5964.
(8) Hirao, A.; Kawasaki, K.; Higashihara, T. *Macromolecules* **2004**, *37*, 5179.
(9) McLeish, T. C. B. *Adv. Phys.* **2002**, *51*, 1379.
(10) McLeish, T. C. B.; Allgaier, J.; Bick, D. K.; Bishko, G.; Biswas, P.; Blackwell, R.; Blottière, B.; Clarke, N.; Gibbs, B.; Groves, D. J.; Hakiki, A.; Heenan, R.; Johnson, J. M.; Kant, R.; Read, D. J.; Young, R. N. *Macromolecules* **1999**, *32*, 6734.
(11) Meissner, J. *Pure. Appl. Chem.* **1975**, *42*, 553.
(12) Bird, R. B.; Armstrong, R. C.; Hassager, O. *Dynamics of Polymeric Liquids, Fluid Mechanics*, 2nd ed.; Wiley-Interscience: New York, 1987; Vol. *1*.
(13) McLeish, T. C. B.; Larson, R. G. *J. Rheol.* **1998**, *42*, 81.
(14) Doufas, A. K.; McHugh, A. J.; Miller, C. *J. Non-Newtonian Fluid Mech.* **2000**, *92*, 27; ibid. 92, 81.
(15) Romero, O. J.; Scriven, L. E.; Carvalho, M. S. *J. Non-Newtonian Fluid Mech.* **2006**, *138*, 63.
(16) Housiadas, K. D.; Klidis, G.; Tsamopoulos, J. *J. Non-Newtonian Fluid Mech.* **2007**, *141*, 193.
(17) Doi, M.; Edwards, S. F. *The Theory of Polymer Dynamics*; Clarendon Press: Oxford, 1986.
(18) Coelho, P. M.; Pinho, F. T. *J. Non-Newtonian Fluid Mech.* **2003**, *110*, 143; 2003, 110, 177.
(19) Yoon, D. Y.; Vacatello, M.; Smith, G. D. In *Monte Carlo and Molecular Dynamics Simulations in Polymer Science*; Binder, K., Ed.; Oxford University Press: New York, 1995.
(20) Allen, M. P.; Tildesley, D. J. *Computer Simulation of Liquids*; Clarendon Press: Oxford, 1987.
(21) Frenkel, D.; Smit, B. *Understanding Molecular Simulation*, 2nd ed.; Academic Press: London, 2002.
(22) Kremer, K.; Binder, K. *Comput. Phys. Rep.* **1988**, *7*, 259.
(23) Kremer, K.; Grest, G. S. *J. Chem. Phys.* **1990**, *92*, 5057.
(24) Baig, C.; Edwards, B. J.; Keffer, D. J.; Cochran, H. D.; Harmandaris, V. A. *J. Chem. Phys.* **2006**, *123*, 084902.
(25) Mavrantzas, V. G. Monte Carlo Simulation of Chain Molecules. In *The Encyclopedia of Modeling for Advanced Materials*; Yip, S., Ed.; Marcel Dekker: New York, 2004.
(26) de Pablo, J. J.; Laso, M.; Suter, U. W. *J. Chem. Phys.* **1992**, *96*, 2395.
(27) Siepmann, I. J.; Frenkel, D. *Mol. Phys.* **1992**, *75*, 59.
(28) Dodd, L. R.; Boone, T. D.; Theodorou, D. N. *Mol. Phys.* **1993**, *78*, 961.
(29) Leontidis, E.; de Pablo, J. J.; Suter, U. W. *Adv. Polym. Sci.* **1994**, *116*, 283.
(30) Pant, P. V. K.; Theodorou, D. N. *Macromolecules* **1995**, *28*, 7224.
(31) Mavrantzas, V. G.; Boone, T. D.; Zervopoulou, E.; Theodorou, D. N. *Macromolecules* **1999**, *32*, 5072.
(32) Uhlherr, A.; Leak, S. J.; Adam, N. E.; Nyberg, P. E.; Doxastakis, M.; Mavrantzas, V. G.; Theodorou, D. N. *Comput. Phys. Commun.* **2002**, *144*, 1.
(33) Karayiannis, N. C.; Mavrantzas, V. G.; Theodorou, D. N. *Phys. Rev. Lett.* **2002**, *88*, 105503.
(34) Karayiannis, N. C.; Giannousaki, A. E.; Mavrantzas, V. G.; Theodorou, D. N. *J. Chem. Phys.* **2002**, *117*, 5465.
(35) Theodorou, D. N. Variable-connectivity Monte Carlo algorithms for the atomistic simulation of long-chain polymer systems. In *Bridging Time Scales: Molecular Simulations for the Next Decade*; Nielaba, P., Mareschal, M., Ciccotti, G., Eds.; Springer-Verlag: Berlin, 2002.
(36) Karayiannis, N. C.; Giannousaki, A. E.; Mavrantzas, V. G. *J. Chem. Phys.* **2003**, *118*, 2451.
(37) Sides, S. W.; Grest, G. S.; Stevens, M. J.; Plimpton, S. J. *J. Polym. Sci., Part B: Polym. Phys.* **2004**, *42*, 199.
(38) Daoulas, K. Ch.; Harmandaris, V. A.; Mavrantzas, V. G. *Macromolecules* **2005**, *38*, 5780.
(39) Peristeras, L. D.; Economou, I. G.; Theodorou, D. N. *Macromolecules* **2005**, *38*, 386.
(40) Ramos, J.; Peristeras, L. D.; Theodorou, D. N. *Macromolecules* **2007**, *40*, 9640.
(41) Alexiadis, O.; Daoulas, K. Ch.; Mavrantzas, V. G. *J. Phys. Chem. B* **2008**, *112*, 1198.
(42) Olaj, O. F.; Lantschbauer, W. *Makromol. Chem., Rapid Commun.* **1982**, *3*, 847.
(43) Harmandaris, V. A.; Mavrantzas, V. G. Molecular Dynamics Simulations of Polymers. In *Simulation Methods for Modeling Polymers*; Theodorou, D. N., Kotelyanskii, M. J., Eds.; Marcel Dekker: New York, 2002.
(44) Harmandaris, V. A.; Mavrantzas, V. G.; Theodorou, D. N.; Kröger, M.; Ramirez, J.; Öttinger, H. C.; Vlassopoulos, D. *Macromolecules* **2003**, *36*, 1376.
(45) Karayiannis, N. C.; Mavrantzas, V. G. *Macromolecules* **2005**, *38*, 8583.
(46) Martin, M. G.; Siepmann, J. I. *J. Phys. Chem. B* **1999**, *103*, 4508.
(47) Rosenbluth, M. N.; Rosenbluth, A. W. *J. Chem. Phys.* **1955**, *23*, 356.
(48) Daoulas, K. C.; Terzis, A. F.; Mavrantzas, V. G. *Macromolecules* **2003**, *36*, 6674.
(49) Fetters, L. J.; Lohse, D. J.; Richter, D.; Witten, T. A.; Zirkel, A. *Macromolecules* **1994**, *27*, 4639.
(50) Lohse, D. J. *J. Macromol. Sci., Part C: Polym. Rev.* **2005**, *45*, 289.
(51) Zimm, B. H.; Stockmayer, W. H. *J. Chem. Phys.* **1949**, *17*, 1301.
(52) Lipson, J. E. G.; Gaunt, D. S.; Wilkinson, M. K.; Whittington, S. G. *Macromolecules* **1987**, *20*, 186.
(53) Freire, J. J. *Adv. Polym. Sci.* **1999**, *143*, 35.
(54) Ramachandran, R.; Beaucage, G.; Kulkarni, A. S.; McFaddin, D.; Merrick-Mack, J.; Galiatsatos, V. *Macromolecules* **2008**, *41*, 9802.
(55) Šolc, K.; Stockmayer, W. H. *J. Chem. Phys.* **1971**, *54*, 2756.
(56) Theodorou, D. N.; Suter, U. W. *Macromolecules* **1985**, *18*, 1206.
(57) Mavrantzas, V. G.; Theodorou, D. N. *Macromolecules* **1998**, *31*, 6310.
(58) Baig, C.; Mavrantzas, V. G. *J. Chem. Phys.* **2009**, accepted.
(59) Zacharopoulos, N.; Economou, I. G. *Macromolecules* **2002**, *35*, 1814.
(60) Zhou, Q.; Larson, R. G. *Macromolecules* **2007**, *40*, 3443.
(61) Tanis, I.; Tragoudaras, D.; Karatasos, K.; Anastasiadis, S. H. *J. Phys. Chem. B* **2009**, *113*, 5356.